
ANDERSON MIXING IN BURES WASSERSTEIN SPACE OF GAUSSIAN MEASURES

Vitalii Aksenov

WIAS

Berlin, Germany

vitalii.aksenov@wias-berlin.de

Martin Eigel

WIAS

Berlin, Germany

martin.eigel@wias-berlin.de

Mathias Oster

RWTH

Aachen, Germany

oster@igpm.rwth-aachen.de

January 30, 2026

ABSTRACT

Various statistical tasks, including sampling or computing Wasserstein barycenters, can be reformulated as fixed-point problems for operators on probability distributions. Accelerating standard fixed-point iteration schemes provides a promising novel approach to the design of efficient numerical methods for these problems. The Wasserstein geometry on the space of probability measures, although not precisely Riemannian, allows us to define various useful Riemannian notions, such as tangent spaces, exponential maps and parallel transport, motivating the adaptation of Riemannian numerical methods. We demonstrate this by developing and implementing the Riemannian Anderson Mixing (RAM) method for Gaussian distributions. The method reuses the history of the residuals and improves the iteration complexity, and we argue that the additional costs, compared to Picard method, are negligible. We show that certain open balls in the Bures-Wasserstein manifold satisfy the requirements for convergence of RAM. The numerical experiments show a significant acceleration compared to a Picard iteration, and performance on par with Riemannian Gradient Descent and Conjugate Gradient methods.

1 Introduction

There is a plethora of tasks in statistics, ranging from sampling given a Bayesian posterior to calculating Wasserstein barycenters and medians, that can be reformulated as a fixed-point problem in Wasserstein space.

For example, the dynamics of the Wasserstein gradient flow of certain functionals is contractive and, thus, induces fix point schemes. To make this more precise, let $\mathcal{P}_2(\mathbb{R}^d)$ be the space of probability measures with finite second moments

$$\mathcal{P}_2(\mathbb{R}^d) := \{\mu : \mathbb{E}_{x \sim \mu} \|x\|_2^2 < \infty\}$$

endowed with the 2-Wasserstein distance

$$W_2^2(\mu_1, \mu_2) := \min_{\pi \in \Pi(\mu_1, \mu_2)} \int \|x - y\|^2 d\pi(x, y),$$

where $\Pi(\mu_1, \mu_2)$ denotes the set of probability distributions on $\mathbb{R}^d \times \mathbb{R}^d$ with marginals μ_1 and μ_2 .

As shown in [1], if some functional $\mathcal{E} : \mathcal{P}_2(\mathbb{R}^d) \rightarrow \mathbb{R} \cup \{\infty\}$ is λ -convex along generalized geodesics for $\lambda > 0$, then for any $\mu \in \overline{D(\mathcal{E})} := \overline{\{\mu \in \mathcal{P}_2(\mathbb{R}^d) : \mathcal{E}(\mu) < \infty\}}$ there exists a unique locally Lipschitz curve $S[\mu](t) : (0, +\infty) \rightarrow$

$\mathcal{P}_2(\mathbb{R}^d)$, which is a gradient flow of \mathcal{E} with initial value μ . For a fixed time τ , the operator defined by $G_\tau(\mu) = S[\mu](\tau)$ satisfies the following contraction estimate:

$$W_2(G_\tau(\mu_1), G_\tau(\mu_2)) \leq e^{-\tau\lambda} W_2(\mu_1, \mu_2).$$

If $\mathcal{E} = \text{KL}(\cdot | \rho_*)$ is the Kullback-Leibler divergence and $\rho_* \sim e^{-V}$ for some coercive potential V , then λ -convexity along generalized geodesics is equivalent to λ -convexity of V and ρ_* is a fixed point of G . The case of KL divergence is of particular interest, as a multitude of numerical algorithms for sampling can be interpreted as relaxations and approximations of this gradient flow. Important examples are Langevin dynamics, see, e.g., [2], and Stein variational gradient descent, see, e.g., [3, 4].

Furthermore, MCMC methods such as Metropolis-Hastings ([5]) or Metropolis-adjusted Langevin dynamics ([6]) have by design the target distribution as an invariant distribution of the Markov chain. Thus, they can also be seen as a fixed-point iteration. In addition, fixed-point iterations can be used to find the Wasserstein Barycenter as noted in [7].

Finally, it is known that for a convex function $f : \mathbb{R}^d \rightarrow \mathbb{R}$, a fixed point of $\text{Id} - h\nabla f$ is the root of the gradient and, therefore, the global minimizer. Thus, a fixed-point method can be used as a first-order optimization method and can be applied to a variety of optimization problems.

However, in various instances fixed-point schemes based on a contraction principle suffer from a slow convergence rate, for example if the contraction constant is close to unity. In order to speed up the calculations one can generalize Euclidean or Riemannian acceleration schemes to Wasserstein space by exploiting the manifold-like structure. Previously, similar ideas have been applied in gradient-based optimization. In [8], the Frank-Wolfe method is adapted to the Wasserstein setting. A Riemannian Frank-Wolfe method was applied to Wasserstein the barycenter problem in [9]. A counterpart of Nesterov acceleration in Wasserstein space is considered in [10, 11]. Riemannian minimization on the Bures-Wasserstein manifold is studied in [12].

It is known that the space of probability measures on \mathbb{R}^d can be endowed with the 2-Wasserstein metric and then forms a complete separable metric space ([1] Proposition 7.1.5). This space is not exactly Riemannian (i.e. there is no atlas of maps to subsets of a fixed linear space), but nevertheless all the important geometric notions, such as geodesics, tangent space, exponential mapping and parallel transport, can be defined. However, the deviations of the geometry from standard Riemannian assumptions, e.g. the exponential map having a vanishing injectivity radius [13], pose hurdles in designing schemes in Wasserstein space beyond the Gaussian case based on already known algorithms.

Contributions: We adapt the Riemannian Anderson Mixing (RAM) algorithm introduced in [14] to Gaussian measures in Bures-Wasserstein manifolds (referred to as BWRAM), verifying some assumptions for the convergence analysis of RAM and identifying the limits of generalizing the methods to general measures in Wasserstein space. The convergence result that we prove can be summarized as follows:

Theorem 1 (Convergence of BWRAM (informal statement)). *Let $G(\Sigma) = \text{Exp}_\Sigma(-F(\Sigma))$ be a contractive mapping on the Bures-Wasserstein manifold and $\Sigma_* \succeq \lambda \text{Id}$ its fixed point with $\lambda > 0$. If the initial iterate $\Sigma_0 \in B_{W_2}(\Sigma_*, r)$ for a sufficiently small r , and under additional smoothness assumptions on F , then the following convergence rate holds*

$$W_2(\Sigma_k, G(\Sigma_k)) \leq [(1 - \beta_k) + \kappa\beta_k] \|r_k\| + \sum_{i=0}^{\max\{m, k\}} \mathcal{O}(\|r_{k-i}\|^2), \quad (1)$$

where Exp denotes the Riemannian exponential map, $r_k = -F(\Sigma_k)$ the fixed-point residual, m the maximal number of historical vectors and $\beta_k > 0$ is the relaxation parameter.

The theoretical estimate says that, up to higher-order terms, the method is guaranteed to converge as good as Picard iteration. We argue that the additional computation costs incurred by the method are negligible in comparison with the operator evaluation, and thus overall speedup of the solution is provided. The improved convergence behavior of BWRAM in comparison to Picard is illustrated with various numerical examples such as estimation of the steady-state of the Ornstein-Uhlenbeck process, minimization of the Kullback-Leibler divergence, and accelerated solution of averaging problems, such as Wasserstein barycenters and geometric medians. We also demonstrate that our method outperforms other well-known Riemannian minimization methods, such as Riemannian Gradient descent and Conjugate Gradient.

Limitations: The method achieves convergence speed superior to Picard iteration at the expense of additional memory costs and a solution of a small-scale minimization problem. The performance of the method is sensitive to the choice of hyperparameters, such as the number of history vectors. Although the Picard method is outperformed robustly for an arbitrary selection, the maximal performance is only achieved for particular values, which cannot be known in advance. In \mathbb{R}^d , there exist strategies to mitigate the issue, for example, adaptive restarting, see, e.g., [15] and regularization, see, e.g., [16]. Their adaptation is left out to future work.

Outline: The paper is structures as follows: In section 2 we recall the Anderson mixing algorithm in Euclidean and Riemannian spaces. Thereafter, we analyze the convergence behavior of the Anderson mixing on Bures-Wasserstein space based on [14] while providing the proofs in the appendix. Finally, in section 5 numerical experiments are shown. The implementation of the method can be accessed at <https://github.com/vivianxenov/fpw>

2 Anderson mixing in Euclidean space and for Riemannian manifolds with bounded sectional curvature

Anderson mixing (AM) ([17]) reuses previous calculations in order to accelerate fixed-point iterations. Given the problem of finding x such that $x = G(x)$ for some operator $G : \mathbb{R}^d \rightarrow \mathbb{R}^d$, at each iteration k , AM uses the history of m previous iterates $\{x_{k-i}\}_{i=0}^{m-1}$ and the values of the operator $g_i = G(x_i)$ to choose the next iterate by a linear combination of the histories and current update candidate. The coefficients are determined by finding weights $\{v_i\}_{i=1}^{m+1}$ such that $\left\| \sum_{i=1}^{m+1} v_i r_{k-i} \right\|_2$ is minimized. In a linear space \mathbb{R}^d , it takes the form of Algorithm 1. Note that the method

Algorithm 1 Anderson mixing in \mathbb{R}^d

Parameters: $x_0 \in \mathbb{R}^d$, relaxation parameters $0 \leq \beta_k \leq 1$, and memory parameter $m \geq 1$.

Returns: A sequence x_0, x_1, \dots , intended to converge to a fixed-point of $G : \mathbb{R}^d \rightarrow \mathbb{R}^d$.

1: **for** $k = 0, 1, \dots$ until convergence **do**

2: Compute $R_k = (r_{k-m}, \dots, r_k)$, where $r_i = G(x_i) - x_i$.

3: Solve

$$\alpha^{(k)} = \arg \min_{v \in \mathbb{R}^{m+1}} \left\{ \|R_k v\|_2 \quad \text{s.t.} \quad \sum_{i=0}^m v_i = 1 \right\}. \quad (2)$$

4: Set

$$x_{k+1} = (1 - \beta_k) \sum_{i=0}^m \alpha_i^{(k)} x_{k-m+i} + \beta_k \sum_{i=0}^m \alpha_i^{(k)} G(x_{k-m+i}). \quad (3)$$

5: **end for**

can be reformulated using residuals $r_k = g_k - x_k$, such that finding the fixed-point is equivalent to setting the residual to zero. Introducing a shorthand notation for the forward finite difference

$$\Delta r_k = r_{k+1} - r_k, \quad \Delta x_k = x_{k+1} - x_k, \quad (4)$$

and the matrices

$$X_k = [\Delta x_{k-m}, \Delta x_{k-m+1}, \dots, \Delta x_{k-1}], \quad (5)$$

$$R_k = [\Delta r_{k-m}, \Delta r_{k-m+1}, \dots, \Delta r_{k-1}], \quad (6)$$

$$\Gamma = \left(\gamma_{k-m}^{(k)}, \dots, \gamma_{k-1}^{(k)} \right)^T, \quad (7)$$

the Anderson mixing in \mathbb{R}^d can be rewritten as

$$\begin{cases} \Gamma_k = \arg \min_{\Gamma} \|r_k - R_k \Gamma\|_2, \\ \bar{r}_k = r_k - R_k \Gamma_k, \\ x_{k+1} = x_k - X_k \Gamma_k + \beta_k \bar{r}_k. \end{cases} \quad (8)$$

In the Euclidean setting, AM is reported to provide significant numeric advantage in comparison to Picard iteration, see [18, 19] and references therein. Observe that the convergence analysis ([20]) in the Euclidean setting yields the estimate

$$\|r_{k+1}\| \leq \frac{\|\bar{r}_k\|}{\|r_k\|} (1 - \beta + \beta \kappa) \|r_k\| + \sum_{i=0}^{m_k} \mathcal{O}(\|r_{k+i}\|^2).$$

where $\frac{\|\bar{r}_k\|}{\|r_k\|} \leq 1$. In the Riemannian setting we can not expect better results. As the manifold has no linear structure, differences of the residuals are not well defined. In order to generalize AM to Riemannian manifolds, the definitions of

Δr_k and Δx_k need to be adapted. One needs to transport tangent vectors from the tangent space of previous iterates to the tangent spaces at the current iterate. Therefore, a suitable vector transport has to be defined on the tangent bundle in order to allow linear combinations. Additionally, the update needs to be approximated by a retraction mapping to stay on the manifold.

The Riemannian version of Anderson mixing (RAM), incorporating these ideas as introduced in [14]. Therein, the authors work in the setting where the operator takes the form

$$G(x) := \text{Exp}_x(-F(x)) \quad (9)$$

for some vector field $F : x \mapsto \text{Tan}_{\mathcal{M}}(x)$. One can see that in such a setting that x_* is a fixed-point if and only if $F(x_*) = 0$. The method is summarized in Algorithm 2 with the vector transport $\mathcal{T}_y^x : T_y \mathcal{M} \rightarrow T_x \mathcal{M}$ and the retraction mapping $\mathcal{R}_x : T_x \mathcal{M} \rightarrow \mathcal{M}$.

Algorithm 2 Riemannian Anderson mixing method

Parameters: $x_0 \in \mathcal{M}, \epsilon, \beta_k > 0, m \in \mathbb{N}^*, k = 1$.

$r_0 = -F(x_0)$ and $x_1 = \mathcal{R}_{x_0}(r_0)$.

while $\|F(x_k)\| \geq \epsilon$ **do**

$m_k = \min\{m, k\}$.

$\Delta x_{k-i}^{(k)} = \mathcal{T}_{x_{k-1}}^{x_k} \Delta x_{k-i}^{(k-1)} \in \text{Tan}_{x_k} \mathcal{M}, i = 1, \dots, m_k$.

$\Delta r_{k-1}^{(k)} = r_k - \mathcal{T}_{x_{k-1}}^{x_k} r_{k-1} \in \text{Tan}_{x_k} \mathcal{M}$.

if $k \geq 2$ **then**

$\Delta r_{k-i}^{(k)} = \mathcal{T}_{x_{k-1}}^{x_k} \Delta r_{k-i}^{(k-1)} \in \text{Tan}_{x_k} \mathcal{M}, i = 2, \dots, m_k$.

end if

$X_k = [\Delta x_{k-m_k}^{(k)}, \dots, \Delta x_{k-1}^{(k)}], R_k = [\Delta r_{k-m_k}^{(k)}, \dots, \Delta r_{k-1}^{(k)}]$.

$r_k = -F(x_k)$.

$\Gamma_k = \arg \min_{\Gamma \in \mathbb{R}^{m_k}} \|r_k - R_k \Gamma\|$.

$\bar{r}_k = r_k - R_k \Gamma_k \in \text{Tan}_{x_k} \mathcal{M}, \Delta x_k^{(k)} = -X_k \Gamma_k + \beta_k \bar{r}_k \in \text{Tan}_{x_k} \mathcal{M}$.

$x_{k+1} = \mathcal{R}_{x_k}(\Delta x_k^{(k)}), k = k + 1$.

end while

3 The Bures-Wasserstein space of Gaussians

3.1 Geometric notions

The set of Gaussian measures forms a sub-manifold of the «manifold» of probability measures with bounded second moment $\mathcal{P}_2(\mathbb{R}^d)$ with respect to the Wasserstein metric, see, e.g., [21, 22, 23]. The advantage of this restriction is that many geometric notions such as parallel transport have a more computationally feasible formulation in terms of matrix equations in the Gaussian setting than in the general case.

We define the set of all Gaussians with zero mean as $\mathcal{N}_0^d = \{\mathcal{N}(0, \Sigma), 0 \prec \Sigma \in \mathbb{R}^{d \times d}\}$. The set \mathcal{N}_0^d can be identified with the set $\text{Sym}^{++}(d)$ of symmetric positive-definite matrices (each measure is identified with its covariance matrix Σ). Then the Wasserstein distance between two Gaussian measures can be computed as

$$W_2^2(\mathcal{N}(0, \Sigma_0), \mathcal{N}(0, \Sigma_1)) = \text{Tr} \Sigma_0 + \text{Tr} \Sigma_1 - 2 \text{Tr} \left(\Sigma_0^{1/2} \Sigma_1 \Sigma_0^{1/2} \right)^{1/2}. \quad (10)$$

We will identify $\mathcal{N}(0, \Sigma)$ with Σ synonymously and use $W_2(\Sigma_0, \Sigma_1) = W_2(\mathcal{N}(0, \Sigma_0), \mathcal{N}(0, \Sigma_1))$. Given a linear map T , a Gaussian measure with covariance Σ_0 can be transformed to a new Gaussian with covariance $\Sigma_1 = T \Sigma_0 T^*$ by $x \mapsto Tx$. Reversely, given two covariances $\Sigma_{0,1}$ there is an optimal linear map T that transforms the Gaussians into each other. It can be computed as the unique positive solution of the Riccati equation

$$\Sigma_1 = T \Sigma_0 T^*, \quad T = \Sigma_1^{1/2} \left(\Sigma_1^{1/2} \Sigma_0 \Sigma_1^{1/2} \right)^{-1/2} \Sigma_1^{1/2}.$$

For two measures with parameters $(0, \Sigma_{0,1})$ consider the convex function

$$\mathcal{W}(x) = \frac{1}{2} \langle x, Tx \rangle \quad (11)$$

where T is the optimal linear map interrelating Σ_0 and Σ_1 . One can see that $(\text{Id}, \nabla W)_{\sharp} \mathcal{N}(0, \Sigma_0)$ is the optimal transport coupling between $\mathcal{N}(0, \Sigma_0)$ and $\mathcal{N}(0, \Sigma_1)$. Furthermore, any point on the geodesic between the measures is also a Gaussian: $\rho_t = \mathcal{N}(0, \Sigma_t)$, $t \in [0, 1]$ and is given by

$$\Sigma_t = ((1-t) \text{Id} + tT) \Sigma_0 ((1-t) \text{Id} + tT). \quad (12)$$

Remark 3.1. One can also analyze Gaussians with non-zero mean m_0, m_1 by adding $\|m_0 - m_1\|^2$ to the distance. Then the linear map T becomes affine and $\mathcal{W}(x) = \frac{1}{2} \langle x - m_0, T(x - m_0) \rangle + \langle x, m_1 \rangle$. The geodesic is augmented by $m_t = (1-t)m_0 + tm_1$.

One key ingredient for adapting Anderson mixing to the manifold setting is the notion of tangent spaces and exponential maps. In [21], the tangent space at $\Sigma \in \mathcal{N}_0^d$ is identified by $\text{Sym}(d)$ with the scalar product and norm given respectively by

$$\langle U, V \rangle_{\Sigma} := \text{Tr } U \Sigma V, \quad \|V\|_{\Sigma}^2 = \text{Tr } V \Sigma V. \quad (13)$$

By the embedding

$$V \in \text{Sym}(d) \mapsto v(x) = Vx \in L^2_{\mathcal{N}(0, \Sigma_0)}(\mathbb{R}^d)$$

$\text{Sym}(d)$ is identified with a subspace to the general tangent space in the Wasserstein space, as defined in [1]. The exponential mapping takes the form

$$\text{Exp}_{\Sigma}(V) := (\text{Id} + V)\Sigma(\text{Id} + V). \quad (14)$$

Note that the exponential map is only well defined for V with limited norm. For example for $V = -\text{Id}$ the result of the exponential map is not positive definite.

3.2 Properties in the neighborhood of a nondegenerate distribution

In order to apply local convergence theory of RAM from [14], one has to know certain properties of the manifold in the neighborhood of the fixed-point. In that regard, we have proven several novel statements, that allow to relate the Bures-Wasserstein distance between the distributions and norms of tangent vectors to Frobenius norms of the symmetric matrices that represent them. This significantly simplifies the subsequent numerical analysis. We summarize our findings in the following theorem:

Theorem 2. Let Σ_* be a nondegenerate covariance matrix, and

$$0 < \lambda_d^* \leq \dots \leq \lambda_1^*$$

be the eigenvalues of Σ_* . Define the Bures-Wasserstein ball as

$$B_r(\Sigma_*) := \{\Sigma \in \mathcal{N}_0^d : W_2(\Sigma, \Sigma_*) \leq r\} \quad (15)$$

and consider $r < \frac{1}{2} \sqrt{\lambda_d^*}$

Then, for $\Sigma, \Sigma_1, \Sigma_2 \in B_r(\Sigma_*)$:

- $B_r(\Sigma_*)$ is compact in \mathcal{N}_0^d .
- Its sectional curvature is uniformly bounded.
- The following estimates hold:

$$(\sqrt{\lambda_d^*} - r) \|V\|_F \leq \|V\|_{\Sigma} \leq (\sqrt{\lambda_1^*} + r) \|V\|_F \quad (16)$$

$$\|V\|_{\Sigma_2} \leq \frac{\sqrt{\lambda_1^*} + r}{\sqrt{\lambda_d^*} - r} \|V\|_{\Sigma_1} \quad (17)$$

$$\|\Sigma_1 - \Sigma_2\|_F \leq 2\sqrt{2}(\sqrt{\lambda_1^*} + \sqrt{\lambda_d^*}) W_2(\Sigma_1, \Sigma_2) \quad (18)$$

- For every $V \in \text{Tan}_{\Sigma} \mathcal{N}_0^d$ such that $\|V\|_{\Sigma} \leq \frac{1}{2}r$, it holds that

$$W_2(\Sigma, \text{Exp}_{\Sigma}(V)) = \|V\|_{\Sigma} \quad \forall \Sigma \in B_r(\Sigma_*) \quad (19)$$

The proof is split into multiple lemmata, which can be found in the Appendix, subsection A.1. The overall idea is to show that a perturbation of the covariance matrix, which is small in terms of the Bures-Wasserstein distance, leads to a small perturbation of the eigenvalues. Uniform bound on the eigenvalues leads to bounded sectional curvature due to the explicit formulas, derived in [21]. Additionally, it allows to compare the tangent norm to the Frobenius norm by (16). As the Frobenius norm does not depend on the current distribution, the dynamic optimal transport can be used to estimate the length of the Bures-Wasserstein geodesic by a Euclidean geodesic with the same endpoints, leading to (18).

Remark 3.2. The property (19) establishes the injectivity of the exponential map in a neighborhood of zero in the tangent space. Together with the sectional curvature bound, these properties are a cornerstone of the convergence analysis of RAM. These properties do not hold for the Wasserstein space of arbitrary measures, rendering the convergence analysis for general measures in Wasserstein space difficult.

3.3 Construction of the vector transport map

A vector transport mapping has to be defined in order to aggregate the historical vectors to in a common tangent space. The requirements on the mapping, sufficient for the convergence of RAM, are given in (4.2). Intuitively, the vector transport mapping can be viewed as an approximation of the parallel transport.

On the space $\mathcal{P}_2(\mathbb{R}^d)$ the parallel transport is defined in [24] along a class of regular curves. The main property of such curves $\rho_t : [0, 1] \mapsto \mathcal{P}_2(\mathbb{R}^d)$, generated by some Lipschitz vector field v_t , is that there exist a family of mappings τ_s^t , such that for arbitrary $s, t \in [0, 1]$

$$\rho_t = (\tau_s^t)_{\sharp} \rho_s$$

and the mappings satisfy the group property, i.e. $\tau_s^p \circ \tau_t^s = \tau_t^p$ and $\tau_s^t = (\tau_t^s)^{-1}$. Then, an isometric map called *vector translation* between L_{2,ρ_t} and L_{2,ρ_s} is defined as $u \mapsto u \circ \tau_s^t$ and the parallel transport is constructed as a limit of the approximation

$$\mathcal{P}_{t_k}^{t_{k+1}} u := \Pi_{\text{Tan}_{\rho_{t_{k+1}}} \mathcal{P}_2(\mathbb{R}^d)} (u \circ \tau_{t_{k+1}}^{t_k}), \quad (20)$$

$$\mathcal{P}[t_0, \dots, t_N]u := \mathcal{P}_{t_{N-1}}^{t_N} \circ \mathcal{P}_{t_{N-2}}^{t_{N-1}} \circ \dots \circ \mathcal{P}_{t_0}^{t_1} u \quad (21)$$

with respect to partitions $0 = t_0 < t_1 < \dots < t_N = 1$ as $\max_k |t_{k+1} - t_k| \rightarrow 0$.

In case of Gaussian measures, the geodesics are regular. As shown in [23], the notion of parallel transport in the sense of [24] then coincides with standard Riemannian parallel transport. This mapping is a natural candidate, satisfying this Assumption 4.2. The ODE for the parallel transport was derived and can be solved numerically with a suitable adaptive ODE solver. However, integrating an ordinary differential equation on the manifold can be more numerically challenging than the original fixed-point problem, making parallel transport unsuitable as a component of the algorithm. Since the assumptions are quite relaxed, it makes sense to explore other options, trading off the exactness of the approximation with computational efficiency.

Firstly, we consider an approximation inspired by the discrete scheme (21) with just *one* timestep for the approximation, i.e.

$$\mathcal{T}_{\Sigma_0}^{\Sigma_1} U := \Pi_{\Sigma_1} (U T_{01}^{-1}), \quad (22)$$

where T_{01} is the matrix of the optimal transport map between Σ_0 and Σ_1 .

Proposition 3.1. $\Pi_{\Sigma_1}(U T_{01}^{-1})$, the projection to the tangent space at Σ_1 , is the unique symmetric solution of the equation

$$\Sigma_1 X + X \Sigma_1 = \Sigma_1 U T_{01}^{-1} + (U T_{01}^{-1})^T \Sigma_1. \quad (23)$$

The proof can be seen in the Appendix, subsection A.3.

The bound $\|\mathcal{T}_{\Sigma_0}^{\Sigma_1} U\|_{\Sigma_1} \leq \|U\|_{\Sigma_0}$ for Assumption 4.2 holds because vector translation is an isometry and because of the property of the orthogonal projection. The approximation is illustrated in Figure 1. Linear map T_{01} pushes

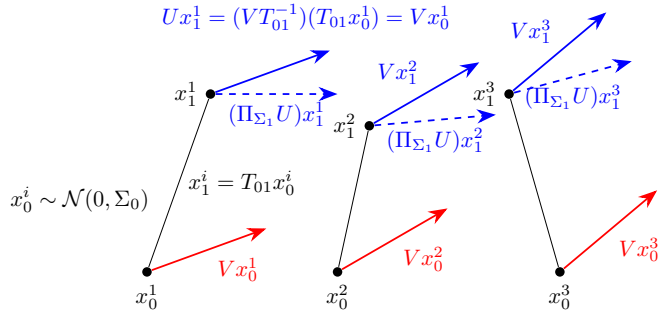


Figure 1: Approximate vector transport along Bures-Wasserstein geodesic

the distribution with covariance Σ_0 forward to the one with covariance Σ_1 . The individual particles move in a straight line: $x_1 = T_{01}x_0$. The vector translation of the vector field $v(x_0) = Vx_0$ is a composition of this move with V , i.e. $U = VT_{01}^{-1}$. Note that $U \in \text{Tan}_{\Sigma_1} \mathcal{N}_0^d$ if and only if V and T_{01}^{-1} commute, which is not the case in general. Thus a projection Π_{Σ_1} is needed. Note that the mapping is well-defined and satisfies the uniform norm bound from Assumption 4.2 with $M = 1$ for the whole \mathcal{N}_0^d .

Secondly, in a local neighborhood of a nondegenerate covariance matrix Σ_* , the identity mapping of $\text{Sym}(\mathbb{R}^d)$ can be viewed as a linear operator between tangent spaces $\text{Id}_{\Sigma_1}^{\Sigma_2} : \text{Tan}_{\Sigma_1} \mathcal{N}_0^d \rightarrow \text{Tan}_{\Sigma_2} \mathcal{N}_0^d$. Due to (17), it also satisfies the bound

$$\left\| \text{Id}_{\Sigma_1}^{\Sigma_2} V \right\|_{\Sigma_2} \leq \frac{\sqrt{\lambda_1^*} + r}{\sqrt{\lambda_d^*} - r} \|V\|_{\Sigma_1} \quad \forall V \in \text{Tan}_{\Sigma_1} \mathcal{N}_0^d$$

which is uniform on the ball $B_r(\Sigma_*)$ with $r < \sqrt{\lambda_d^*}$. This is a perfect candidate from the computational perspective (no computation is needed), but the constant may affect the radius of the method's convergence. We provide the comparison of the vector transport mappings $\mathcal{T}_{\Sigma_1}^{\Sigma_2}$ and $\text{Id}_{\Sigma_1}^{\Sigma_2}$ in section 5.

Remark 3.3. *In this paper, we provide definitions, study the properties and derive numerical algorithms for Riemannian notions such as exponential map, vector transport, projection on the tangent space, etc. These can be used to adapt a broad range of Riemannian numerical methods, such as RGD, RCG, RLBFGS etc. to probabilistic tasks, that can be reformulated as fixed-point or optimization problems. Although in the convergence analysis we have focused on RAM, in the numerical experiments, we also compare its performance to RGD and RCG. Up to our best knowledge, this is the first time these methods are applied in the setting considered.*

4 Riemannian Anderson Mixing on Bures-Wasserstein space

4.1 Convergence

In order to show the convergence of Anderson mixing in Bures-Wasserstein space we follow the lines of [14]. As we have explicit formulas for the parallel transport \mathcal{P} as well as the exponential map some arguments of [14] can be simplified. Hence, we repeat the proof in the appendix. As in the Euclidean case in [25, 26], we impose the «coercive» and «locally Lipschitz continuous» property on the vector field F as well as on its Jacobian H . Define the fixed point map $G(\Sigma) := \text{Exp}_{\Sigma}(-F(\Sigma))$.

Assumption 4.1. *Assume $\Sigma_* \in \mathcal{N}_0^d$ with $\Sigma_* = G(\Sigma_*)$ and let $\lambda_i^* > 0$ be its eigenvalues in decreasing order. Assume there exists a ball $B_r(\Sigma_*)$ with $r < \frac{1}{2}\sqrt{\lambda_d^*}$ and constants $0 < L_1 < L_2$ and $L_H > 0$ such that for all $\Sigma_1, \Sigma_2 \in B_r(\Sigma_*)$ holds:*

$$L_1 W_2(\Sigma_1, \Sigma_2) \leq \|F(\Sigma_1) - \mathcal{P}_{\Sigma_2}^{\Sigma_1} F(\Sigma_2)\|_{\Sigma_1} \leq L_2 W_2(\Sigma_1, \Sigma_2), \quad (24)$$

$$\left\| \mathcal{P}_{\Sigma_2}^{\Sigma_1} H(\Sigma_2) \mathcal{P}_{\Sigma_1}^{\Sigma_2} - H(\Sigma_1) \right\|_{\Sigma_1} \leq L_H W_2(\Sigma_1, \Sigma_2), \quad (25)$$

$$W_2(G(\Sigma_1), G(\Sigma_2)) \leq \kappa W_2(\Sigma_1, \Sigma_2) \text{ for some } \kappa < 1. \quad (26)$$

Assumption 4.2. *The vector transport \mathcal{T} is continuously differentiable and there exists some $M > 0$ such that*

$$\left\| \mathcal{T}_{\Sigma_1}^{\Sigma_2} V \right\|_{\Sigma_2} \leq M \|V\|_{\Sigma_1}$$

for all $\Sigma_1, \Sigma_2 \in B_r(\Sigma_*)$, $\forall V \in \text{Tan}_{\Sigma_1} \mathcal{N}_0^d$.

Observe that for the vector transports we employ we have $M \leq 1$ and $M \leq \frac{\sqrt{\lambda_1^*} + r}{\sqrt{\lambda_d^*} - r}$ respectively.

The final assumption concerns the uniform boundedness of the extrapolation coefficients Γ_k in the RAM method. This assumption is common for analyzing convergence in the Euclidean setting, see [25].

Assumption 4.3. *There exists a positive constant M_{Γ} such that $\|\Gamma_k\|_{\infty} \leq M_{\Gamma}$ for all $k \in \mathbb{N}$.*

Following [14], we can formulate the following theorem.

Theorem 3. *Assume $\{\Sigma_n\}_{n \geq 1}$ is generated by Algorithm 2 and suppose Assumption 4.1-4.3 hold. Additionally, assume that initial point $\Sigma_0 \in \mathcal{N}_0^d$ satisfies $W_2(\Sigma_0, \Sigma_*) \leq \frac{1}{1+L_2} \min \left\{ \frac{r}{L_2(mM_1+\beta+1)}, \frac{L_1-L_2+(1-\kappa)\beta L_2}{MmL_2^2} \right\}$.*

Then for all $k \geq 1$ we have $W_2(\Sigma_k, \Sigma_*) \leq \min \left\{ \frac{r}{L_2(mM_1 + \beta + 1)}, \frac{L_1 - L_2 + (1 - \kappa)\beta L_2}{MmL_2^2} \right\}$ and it holds that

$$\|r_{k+1}\| \leq \theta_k (1 - \beta_k + \kappa\beta_k) \|r_k\| + \sum_{i=0}^{m_k} \mathcal{O}(\|r_i\|^2) \quad \text{where} \quad \theta_k = \frac{\|\bar{r}_k\|}{\|r_k\|} \leq 1. \quad (27)$$

Remark 4.1. The hidden constants in $\sum_{i=0}^{m_k} \mathcal{O}(\|r_i\|^2)$ take the form

$$c_0 \tilde{r} m M_1^2 + M_3 + 2M_\Gamma M_2$$

with

$$M_1 = M_\Gamma \frac{1}{L_1} \max\{M^{m_k} + M^{m_k-1}, M^2 + M\} + 1.$$

In contrast, in [14] the constants read

$$\left((\kappa + 1)(C + \sqrt{K}) + \frac{c_0 \tilde{r}}{2} + \sqrt{K} \max\{1, L_2\} \right) m M_1^2 + m (M_3 + 2M_\Gamma M_3)$$

with

$$M_1 = \max\left\{\frac{M M_\Gamma}{L_1 C} + 1, M_\Gamma \tilde{M}, \tilde{M}\right\}$$

where

$$\tilde{M} = \frac{1}{L_1 C} \max\{M^{m_k} + M^{m_k-1}, M^2 + M\}$$

Since the mapping is assumed to be contractive, the decrease in residual can be directly linked to the distance to the solution

$$\begin{aligned} W(\Sigma_k, \Sigma_*) &\leq W(G(\Sigma_k), \Sigma_*) + W(G(\Sigma_k), \Sigma_k) \leq \kappa W(\Sigma_k, \Sigma_*) + W(G(\Sigma_k), \Sigma_k) \\ W(\Sigma_k, \Sigma_*) &\leq \frac{1}{1 - \kappa} \|r_k\| \end{aligned}$$

The proof can be found in the appendix (A.4) and follows [14] very closely while improving the constants and simplifying some steps for this particular case.

The estimate (27) can be interpreted as follows. The method decreases the residual at least as good as a relaxed Picard iteration (the residual decrease in that case would be exactly $(1 - \beta_k + \kappa\beta_k) \|r_k\|$), up to “higher order terms” $\mathcal{O}(\sum_i \|r_{k-i}\|^2)$. When the iterate is sufficiently close to the solution, the higher order terms can be neglected. The coefficient $\theta_k = \frac{\|\bar{r}_k\|}{\|r_k\|}$ quantifies the gain, compared to the Picard step, and depends on the quality of the solution of the subproblem. The estimate suggests to keep the history length of the method bounded and relatively short. This intuition is indeed backed by our practical experience, where a significant acceleration can be achieved for quite modest history lengths $m \in 1, \dots, 5$. As of now, estimates of such type (i.e. including \mathcal{O} terms) are a state of the art for the case of Anderson Mixing on nonlinear problems even on the Euclidean space (see [27, 28, 15, 20]).

4.2 Examples of operators

In the following we describe several examples of fixed-point problems, suitable for acceleration with BWRAM. We reflect on their contractive properties and and discuss the possible applications.

4.2.1 Ornstein-Uhlenbeck process

The evolution of the Ornstein-Uhlenbeck process is a suitable model problem, since it is known that the induced fixed-point operator is contractive. It is defined by the stochastic differential equation

$$dX_t = -\Sigma_*^{-1} X_t dt + \sqrt{2} dW_t \quad (28)$$

as follows: if $X_0 \sim \mathcal{N}(0, \Sigma_0)$, then for some fixed timestep parameter τ , $G(\Sigma_0)$ is the law of X_τ . The process can be identified with the gradient flow of the Kullback-Leibler divergence $\text{KL}(\cdot | \mathcal{N}(0, \Sigma_*))$ w.r.t. the 2-Wasserstein distance. In case of Gaussians, there is an explicit solution [2]

$$X_\tau \sim e^{-\tau \Sigma_*^{-1}} X_0 + \Sigma_*^{1/2} \left(I - e^{-2\tau \Sigma_*^{-1}} \right)^{1/2} Z,$$

where $Z \sim \mathcal{N}(0, I_d)$. Thus, in case of $X_0 \sim \mathcal{N}(0, \Sigma)$, the covariance after one step is given by

$$G(\Sigma) = e^{-\tau \Sigma_*^{-1}} \Sigma e^{-\tau \Sigma_*^{-1}} + \left(I - e^{-2\tau \Sigma_*^{-1}} \right)^{1/2} \Sigma_* \left(I - e^{-2\tau \Sigma_*^{-1}} \right)^{1/2}. \quad (29)$$

For a symmetric positive definite Σ , the matrices I , Σ , Σ^{-1} , $\Sigma^{1/2}$ and $e^{-2\tau \Sigma^{-1}}$ all have the same basis of eigenvectors thus, commute and it is easy to simplify (29), and verify Σ_* is a fixed point.

4.2.2 Minimization of functionals

Alternatively, the operator can be defined having some vector field F as $G(\Sigma) = \text{Exp}_{\Sigma}(-hF(\Sigma))$. If F is a Wasserstein gradient of some functional,

$$F(\rho) = \partial_W \mathcal{E}(\rho) := \nabla \frac{\delta}{\delta \rho} \mathcal{E}(\rho)$$

one can opt to minimize this functional with fixed-point iteration for the following operator

$$G(\rho) := \text{Exp}_{\rho}(-h\partial_W \mathcal{E}) \quad (30)$$

This fixed-point iteration can be seen as a generalization of the Gradient Descent method to spaces with Riemannian-like geometry. Minimization over the BW space finds applications in Bayesian logistic regression [29, 30], distributional robust optimization [31], etc.

4.2.3 Kullback-Leibler divergence

As a model minimization problem, we consider the Kullback-Leibler divergence:

$$\partial_W (\text{KL}(\mathcal{N}(0, \Sigma) \mid \mathcal{N}(0, \Sigma_*))) (x) = \nabla_x (\log \rho_{\Sigma}(x) - \rho_{\Sigma_*}(x)) = (\Sigma^{-1} - \Sigma_*^{-1})x. \quad (31)$$

The operator can be written as

$$G_h(\Sigma) = \text{Exp}_{\Sigma}(-h\partial_W \text{KL}(\Sigma \mid \Sigma_*)) = (\text{Id} - h(\Sigma^{-1} - \Sigma_*^{-1}))\Sigma(\text{Id} - h(\Sigma^{-1} - \Sigma_*^{-1})), \quad (32)$$

where $h > 0$ is a step-size parameter that can be selected so that the iterative procedure converges.

Theorem 4. *For a nondegenerate Σ_* , there exists a radius r and stepsize parameters τ, h , such that the operators, defined by (29), (32) are contractive on $B_r(\Sigma_*)$*

Proof. According to the theory in [1], the functional $\text{KL}(\cdot \mid \mathcal{N}(0, \Sigma_*))$ is $1/\lambda_1^*$ -convex along generalized geodesics. Thus, the following contraction estimate for the Ornstein-Uhlenbeck process (29) can be given:

$$W_2(G(\Sigma_0), G(\Sigma_1)) \leq e^{-\frac{\tau}{\lambda_1^*}} W_2(\Sigma_0, \Sigma_1). \quad (33)$$

The operator (32) can be seen as a one-step explicit time discretization of the gradient flow (28). If $\Sigma = \Sigma^*$, then $\partial_W \text{KL}(\mathcal{N}(0, \Sigma) \mid \mathcal{N}(0, \Sigma_*)) = 0$ and Σ is a fixed-point. Thus, it is natural to expect that, for sufficiently small stepsize h , the discretization should capture the contractive property of the continuous process. The strict proof relies on establishing a property, analogous to the L -Lipschitz gradient property of a functional in \mathbb{R}^d , in the neighborhood of the fixed-point. It is quite technical, and thus is postponed to the Appendix (subsection A.2). \square

4.3 Complexity analysis

For fixed-point problems in \mathbb{R}^d , the evaluation of $G(x_k)$ typically is the most computationally expensive operation. For example, if Anderson Mixing is used in the context of coupled PDE systems, each evaluation of the operator requires a numerical solution of complicated PDE(s), with parameters defined by the current iterate x_k (see [17, 18, 32] for more examples). The method's efficiency is evaluated by comparing the amount of the number of the operator calls with Picard method. The overhead, induced by the acceleration algorithm can be neglected in this case. Indeed, the additional operations consist of finding the mixing coefficients via (2) and then computing the new iterate by formula (3). The storage of historical vectors requires $\mathcal{O}(md)$ additional memory. The assembly of the matrices, needed to solve (2) can be estimated as $\mathcal{O}(m^2d)$ operations. Additional $\mathcal{O}(m^3)$ operations are required to solve the minimization problem. Since m is a small number in the range $1 \dots 15$, and the complexity of the operator evaluation is expected to scale worse than linear, the neglection of the overhead is justified from the computational complexity perspective, especially for large-scale problems ($d \gg m$).

If the Gaussian distributions in \mathcal{N}_0^d are considered, the total number of the degrees of freedom, needed to represent the points and tangent vectors, is $\mathcal{O}(d^2)$. Thus, the storage of the matrices X_k, R_k requires $\mathcal{O}(md^2)$ memory. In addition to the aforementioned steps, Riemannian Anderson Mixing performs the vector transport. In case when identity map $\text{Id}_{\Sigma_1}^{\Sigma_2}$ is used, there is no computation at all. For the one-step approximation $\mathcal{T}_{\Sigma_1}^{\Sigma_2}$, a computation of the OT map, and m matrix multiplications and solutions of (23) are needed, thus the total number of iterations can estimated as $\mathcal{O}(md^3)$. The computation of the matrices in (34) requires $\mathcal{O}(m^2d^3)$, and the update using Riemannian exponential (14) costs $\mathcal{O}(d^3)$.

For example, in the averaging problems, that we consider in the sequel, the computation of each operator requires computing the optimal transport map between the current distribution and N_{σ} other ones. This can be efficiently

implemented in $\mathcal{O}(N_\sigma d^3)$ operations using the eigenvalue decomposition. In applications, N_σ can be as high as 10^3 [33]. Thus, in our examples the operator computation complexity has the same asymptotic dependence on d , as the overhead introduced by RAM. Nevertheless, we argue that it is possible to achieve overall acceleration when the operator is sufficiently “heavy”, e.g. when N_σ is high.

5 Numerical experiments

The following section provides the implementation details and numeric results. The experiments were performed on a laptop with 13th Gen Intel(R) Core(TM) i7-1355U CPU with 12 cores. The execution time varied from fractions of second in low-dimensional cases up to ~ 100 s for 500 dimensions.

5.1 Implementation details

Since the explicit form of the exponential is given in Equation 14, we can directly use it as the retraction mapping.

To adhere to Assumption 4.3, in the minimization subproblem we impose a bound $l_{\infty, \max}$ for the weights Γ_k , and solve (using cvxpy package [34]) the regularized problem

$$\Gamma_k = \arg \min_{\|\Gamma\|_\infty \leq l_{\infty, \max}} \|r_k - R_k \Gamma\|. \quad (34)$$

5.2 Ornstein-Uhlenbeck process

In the first set of experiments, we accelerate the Picard iteration for the operator (29), defined by the Ornstein-Uhlenbeck process (28). We vary d , σ_{\max} and for each pair, we run the Picard iteration and Anderson acceleration with different lengths of history m , until the residual norm is smaller than $\epsilon = 10^{-6}$. The acceleration measured as $\frac{N_{\text{Picard}}}{N_{\text{AA}}}$ is averaged over $n = 6$ independent covariances. The maximal mean acceleration, depending on d and σ_{\max} , is presented in Table 1a. The improved convergence of BWRAM for the Ornstein-Uhlenbeck problem, in comparison to Picard, RGD and RCG methods, is presented in Figure 2a.

Table 1: Maximal mean acceleration for BWRAM, depending on d and σ_{\max} .

σ_{\max}	1.0	5.0	10.0	20.0	σ_{\max}	5.0	10.0	20.0
d					d			
4	1.62	5.89	8.29	14.16	4	4.09	6.33	10.77
8	1.73	3.68	4.23	5.76	8	3.21	4.22	5.12
16	1.73	4.00	4.76	5.94	16	3.15	4.02	4.89
32	1.73	4.12	4.86	5.41	32	3.13	4.39	4.84
64	1.75	4.33	5.60	6.67	64	3.10	4.61	5.01
128	1.87	4.60	4.78	5.87	128	3.00	4.54	5.20

(a) Ornstein-Uhlenbeck dynamic

(b) KL minimization

5.3 Minimization of KL divergence

We can compare the performance of the BWRAM to minimization methods, in particular, Riemannian Gradient Descent (RGD) and Riemannian Conjugate Gradient (RCG) [35]. The numerical implementation of these methods from the package pymanopt [36] has been used.

The values of Σ_* were chosen in the same way, as for the experiments with the Ornstein-Uhlenbeck dynamic. The scaling parameter $h = 0.3$ was chosen so that every methods converges. Each method is iterated until the Kullback-Leibler divergence is reduced below $\epsilon = 10^{-10}$. The acceleration is averaged for different realizations of Σ_* . The best mean acceleration among different history lengths, depending on d and σ_{\max} , is presented in Table 1b. The improved convergence of BWRAM for the KL minimization problem, in comparison to Picard, RGD and RCG methods, is presented in Figure 2b.

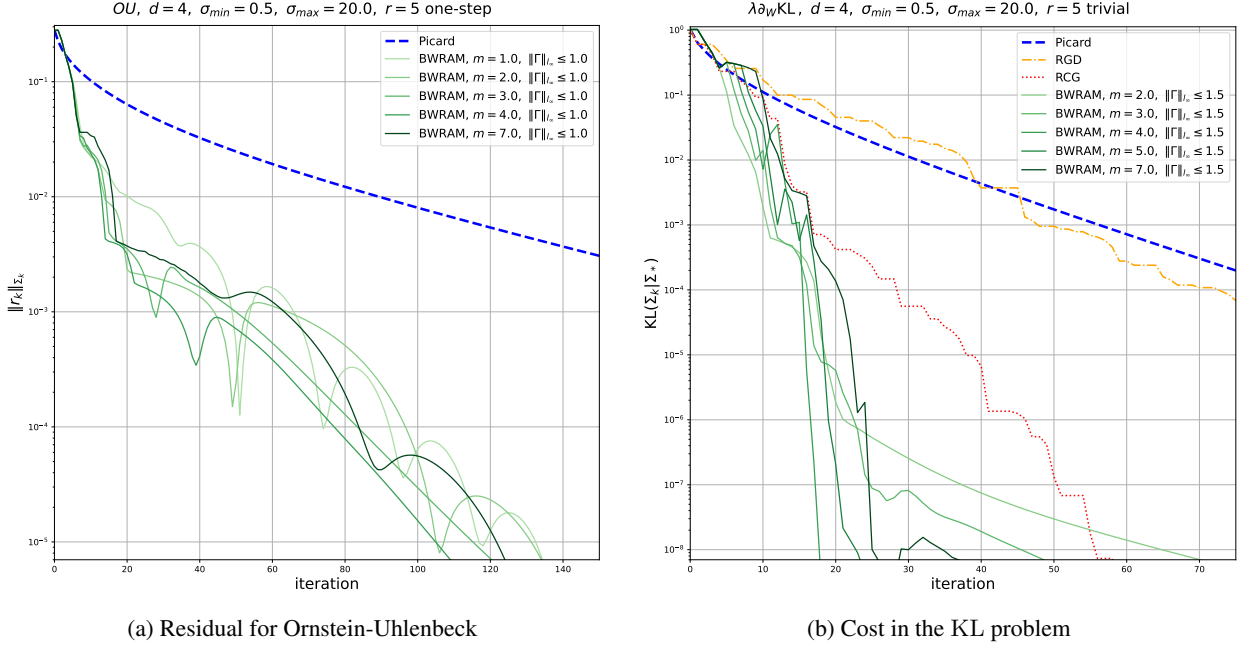


Figure 2: Convergence of BWRAM on model problems, in comparison to Picard (blue), RGD (orange) and RCG (red) methods

5.4 Averaging probability distributions

Averaging data sources is an important problem in machine learning (see, for example, [37] and references therein). In case of averaging probability distributions, a common approach is to consider a Wasserstein barycenter, introduced in [38]. Given k distributions $\{\rho_i \in \mathcal{P}_2(\mathbb{R}^d)\}_{i=1}^k$ and weights $\{\alpha_i > 0 \mid \alpha_1 + \dots + \alpha_k = 1\}$, the Wasserstein barycenter is a minimizer $\min_{\rho \in \mathcal{P}_2(\mathbb{R}^d)} B(\rho)$ of

$$B(\rho) := \sum_{i=1}^{n_\sigma} \alpha_i W_2^2(\rho, \rho_i). \quad (35)$$

In case of absolutely continuous ρ , the Wasserstein gradient of the cost function is given by [33]

$$\partial_W B(\rho) = \sum_{i=1}^{n_\sigma} \alpha_i (T_\rho^{\rho_i} - \text{Id}), \quad (36)$$

where $T_\rho^{\rho_i}$ is the optimal transport map from ρ to ρ_i . The exponential of this gradient defines a fixed-point problem, as noted in [7]. The authors also show that if all ρ_i are absolutely continuous and at least one of them has bounded density, then the barycenter is a fixed-point of this mapping. In case that every ρ_i is a Gaussian, the solution is unique.

Alternative approaches include the *entropy-regularized Wasserstein barycenters* and *Geometric Medians*, which are, respectively, the minimizers of

$$B_\gamma(\rho) := \sum_{i=1}^{n_\sigma} \alpha_i W_2^2(\rho, \rho_i) + \gamma \text{KL}(\rho | \mathcal{N}(0, I_d)) \quad (37)$$

$$M(\Sigma) = \sum_{i=0}^{n_\sigma} \alpha_i W_2(\Sigma, \Sigma_i). \quad (38)$$

The entropic penalty in the first case can be seen as a way to incorporate prior knowledge in the estimation. The geometric median is known to be more robust with respect to the perturbations of the distributions ρ_k , but poses additional difficulty to estimate. In particular, $M(\rho)$ is neither geodesically convex nor geodesically smooth. Given some smoothing parameter $\varepsilon > 0$, we work on a smoothed objective as suggested in [37], namely

$$M_\varepsilon(\rho) = \sum_{i=1}^{n_\sigma} \alpha_i \sqrt{W_2^2(\rho, \rho_i) + \varepsilon^2}. \quad (39)$$

Constraining to the Bures-Wasserstein manifold \mathcal{N}_0^d , the Wasserstein gradients of these objectives are

$$\partial_W B_\gamma(\Sigma) = \sum_{i=1}^{n_\sigma} \alpha_i (T_\Sigma^{\Sigma_i} - \text{Id}) + \gamma (\Sigma^{-1} - \text{Id}), \quad (40)$$

$$\partial_W M_\varepsilon(\Sigma) = \sum_{i=1}^{n_\sigma} \frac{\alpha_i}{\sqrt{W_2(\Sigma, \Sigma_i)^2 + \varepsilon^2}} (T_\Sigma^{\Sigma_i} - \text{Id}). \quad (41)$$

The barycenter problem has been computed with Picard iteration [7] or Riemannian gradient descent [33], which coincide if the gradient step size equals one. Stochastic gradient descent has also been considered [33, 37], with approximation of the sum in Equation 36 by minibatching. For entropic barycenter and median problems, the same methods have been applied e.g. in [37]. To the best of the authors' knowledge, this is a first attempt to apply an accelerated method to such problems.

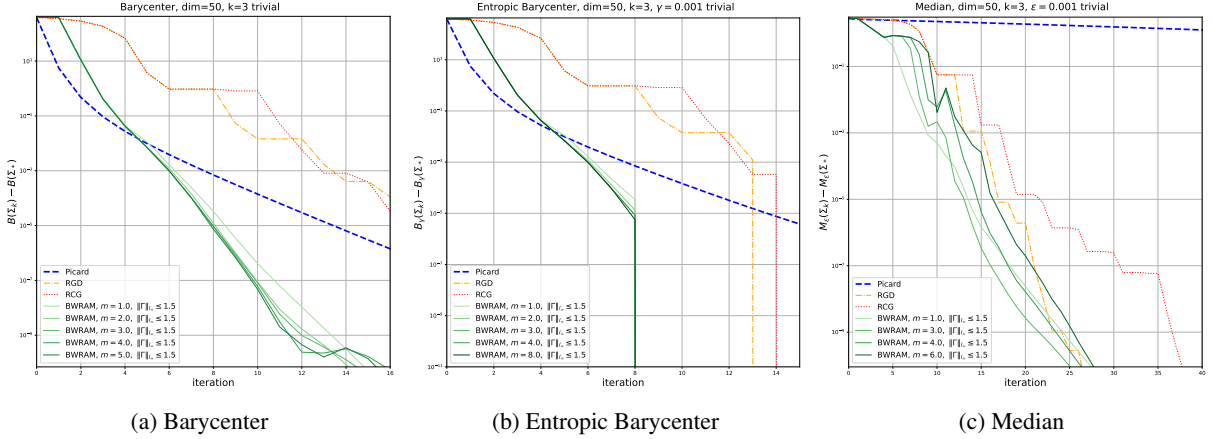


Figure 3: Convergence of the cost. BWRAM (greens) with different history length on the averaging problems, in comparison to Picard (blue), RGD and RCG methods

In Figure 3 one can see that BWRAM outperforms Picard, RGD and RCG for the averaging problems. Details on additional experiments for varying d, n_σ can be found in the appendix.

5.5 Comparison of the vector transport mappings

As noted previously in subsection 4.3, there are several options for the parallel transport mapping. The behavior of

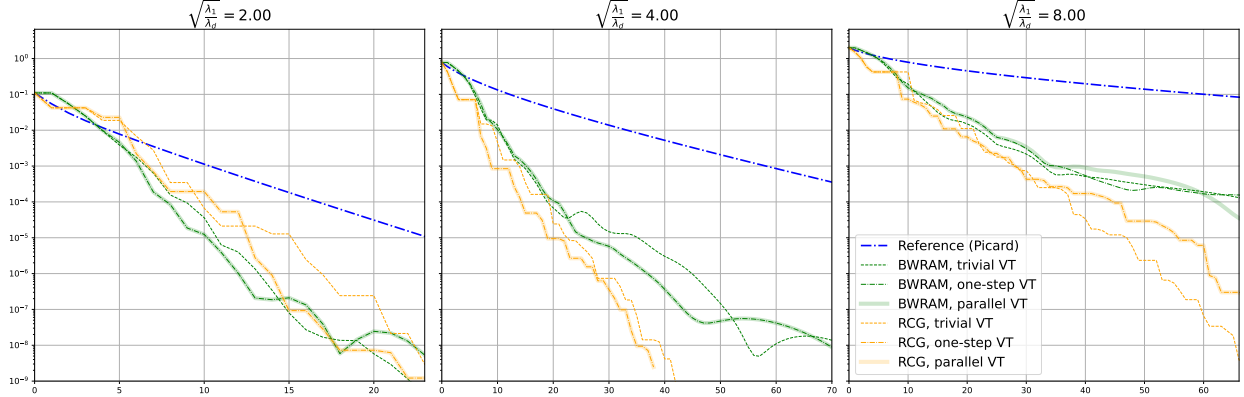


Figure 4: Performance of methods on the KL problem with varying condition number $\sqrt{\lambda_1^* / \lambda_d^*}$. Exact parallel transport, one-step and trivial approximation.

accelerated methods (BWRAM and RCG) with different kinds of vector transport is represented on Figure 4. The computation of the exact parallel transport requires a solution of a nonlinear ODE on the manifold. This iterative procedure could be comparable in numeric complexity to the solution of the fixed-point problem itself. Moreover, in some cases (e.g. the first two illustration), the resulting trajectory of the method is identical to the one with a one-step approximation. These considerations rule out the usage of the exact parallel transport in the practical applications of the method.

The usage of the trivial transport map does not incur any additional computational complexity, in contrast to the one-step approximation, which can increase the per-iteration complexity. On the other hand, in case of trivial transport, the constant M from (4.2) depends on the maximal and minimal eigenvalue ratio in the vicinity of the solution, and can be larger than one. This leads to a decrease of the theoretically guaranteed radius of the ball of converging solutions, and to an increase of the constants, hidden in the \mathcal{O} terms of Theorem 3. Thus, when choosing between one-step and trivial transport map, there exists a tradeoff between the computation efficiency of each iteration and reduced stability of the method and potentially worse acceleration. To assess the effect of this tradeoff in the numerical experiments, we perform a robustness study on a subset of our test cases. The results are presented in the Table 2. We consider

Table 2: Robustness of the performance with respect to different vector transport mappings. KL problem with $\sigma_{\max} = 20$, $\sigma_{\min} = 0.5$ and varying dimension.

d	$\text{Id}_{\Sigma_1}^{\Sigma_2}$		$\mathcal{T}_{\Sigma_1}^{\Sigma_2}$	
	% converged	% accelerated	% converged	% accelerated
4	60.0	53.3	98.8	64.4
8	68.0	54.0	97.3	48.4
16	63.3	53.3	94.1	53.3
32	75.8	66.4	94.7	59.7
64	84.4	74.7	94.9	65.3
128	74.0	66.0	96.4	66.5

the KL minimization problem with fixed maximal and minimal covariance, and vary the dimension. The Anderson method is repeated with a set of varying parameters over several random initializations of the problem as described in subsection 5.3. In this set of test runs, we compute the percentage of runs where the method converged to the prescribed tolerance, and where at least double acceleration was achieved (in comparison with the Picard method). The outcomes show that the usage of trivial transport mapping does negatively affect the convergence. We notice, however, that this is due to divergence of the method on the early stages, which can, in our opinion, be effectively dealt with by incorporating a restarting or early stopping strategy. The probability of acceleration is, however, not changed significantly. We have also performed experiments, evaluating the maximal mean acceleration and best number of iterations, as in the previous sections, with the both mentioned types of vector transport. The results were qualitatively the same, although the particular best values of the hyperparameters do not have to coincide. We thus argue that usage of the trivial vector transport is justified, and claim that BWRAM does improve the iteration complexity with a negligible increase of the per-iteration cost.

6 Conclusion and outlook

The numerical evidence suggests that Anderson mixing performs comparably to established Riemannian minimization methods, while being applicable to a broader set of problems outperforming Picard iteration. The theoretical analysis certifies the local convergence of the method and highlights the geometric structure of the Bures-Wasserstein space. It also outlines the difficulties that have to be overcome in the future work on generalizing the method to arbitrary distributions.

Acknowledgement

VA acknowledges the support of the EMPIR project 20IND04-ATMOC. This project (20IND04 ATMOC) has received funding from the EMPIR programme co-financed by the Participating States and from the European Union’s Horizon 2020 research and innovation programme. ME was supported by ANR-DFG project “COFNET” and DFG SPP 2298 “Theoretical Foundations of Deep Learning”.

MO has received funding by the Deutsche Forschungsgemeinschaft (DFG, German Research Foundation) – project number 442047500 – through the Collaborative Research Center “Sparsity and Singular Structures” (SFB 1481).

Conflict of Interest Statement

The authors have no conflicts of interest to declare related to this publication.

References

- [1] Luigi Ambrosio, Nicola Gigli, and Giuseppe Savaré. *Gradient flows: in metric spaces and in the space of probability measures*. Springer Science & Business Media, 2005.
- [2] Andre Wibisono. Sampling as optimization in the space of measures: The Langevin dynamics as a composite optimization problem. In *Conference on Learning Theory*, pages 2093–3027. PMLR, 2018.
- [3] Qiang Liu and Dilin Wang. Stein variational gradient descent: A general purpose Bayesian inference algorithm. *Advances in neural information processing systems*, 29, 2016.
- [4] Andrew Duncan, Nikolas Nüsken, and Lukasz Szpruch. On the geometry of Stein variational gradient descent. *Journal of Machine Learning Research*, 24(56):1–39, 2023.
- [5] W. K. Hastings. Monte Carlo sampling methods using Markov chains and their applications. *Biometrika*, 57(1):97–109, 04 1970.
- [6] Gareth O. Roberts and Richard L. Tweedie. Exponential convergence of Langevin distributions and their discrete approximations. *Bernoulli*, 2(4):341 – 363, 1996.
- [7] Pedro C Álvarez-Esteban, E Del Barrio, JA Cuesta-Albertos, and C Matrán. A fixed-point approach to barycenters in Wasserstein space. *Journal of Mathematical Analysis and Applications*, 441(2):744–762, 2016.
- [8] Carson Kent, Jiajin Li, Jose Blanchet, and Peter W Glynn. Modified Frank Wolfe in probability space. *Advances in Neural Information Processing Systems*, 34:14448–14462, 2021.
- [9] Melanie Weber and Suvrit Sra. Riemannian optimization via Frank-Wolfe methods. *Mathematical Programming*, 199(1):525–556, 2023.
- [10] Chang Liu, Jingwei Zhuo, Pengyu Cheng, Ruiyi Zhang, Jun Zhu, and Lawrence Carin. Accelerated first-order methods on the Wasserstein space for Bayesian inference. *stat*, 1050:4, 2018.
- [11] Shi Chen, Qin Li, Oliver Tse, and Stephen J Wright. Accelerating optimization over the space of probability measures. *Journal of Machine Learning Research*, 26(31):1–40, 2025.
- [12] Andi Han, Bamdev Mishra, Pratik Kumar Jawanpuria, and Junbin Gao. On riemannian optimization over positive definite matrices with the Bures-Wasserstein geometry. *Advances in Neural Information Processing Systems*, 34:8940–8953, 2021.
- [13] Nicola Gigli. On the geometry of the space of probability measures in \mathbb{R}^n endowed with the quadratic optimal transport distance. 2008.
- [14] Zanyu Li and Chenglong Bao. Riemannian Anderson mixing methods for minimizing C^2 -functions on Riemannian manifolds. *arXiv preprint arXiv:2309.04091*, 2023.
- [15] Fuchao Wei, Chenglong Bao, Yang Liu, and Guangwen Yang. Convergence analysis for restarted Anderson mixing and beyond. *arXiv preprint arXiv:2307.02062*, 2023.
- [16] Fuchao Wei, Chenglong Bao, and Yang Liu. Stochastic anderson mixing for nonconvex stochastic optimization. *Advances in Neural Information Processing Systems*, 34:22995–23008, 2021.
- [17] Haw-ren Fang and Yousef Saad. Two classes of multisecant methods for nonlinear acceleration. *Numerical linear algebra with applications*, 16(3):197–221, 2009.
- [18] Vitalii Aksenov, Maxim Chertov, and Konstantin Sinkov. Application of accelerated fixed-point algorithms to hydrodynamic well-fracture coupling. *Computers and Geotechnics*, 129:103783, 2021.
- [19] Homer F Walker and Peng Ni. Anderson acceleration for fixed-point iterations. *SIAM Journal on Numerical Analysis*, 49(4):1715–1735, 2011.
- [20] Claire Evans, Sara Pollock, Leo G Rebholz, and Mengying Xiao. A proof that anderson acceleration improves the convergence rate in linearly converging fixed-point methods (but not in those converging quadratically). *SIAM Journal on Numerical Analysis*, 58(1):788–810, 2020.

- [21] Asuka Takatsu. On wasserstein geometry of Gaussian measures. *Probabilistic approach to geometry*, 57:463–472, 2010.
- [22] Asuka Takatsu. Wasserstein geometry of Gaussian measures. 2011.
- [23] Luigi Malagò, Luigi Montrucchio, and Giovanni Pistone. Wasserstein riemannian geometry of Gaussian densities. *Information Geometry*, 1:137–179, 2018.
- [24] Luigi Ambrosio and Nicola Gigli. Construction of the parallel transport in the Wasserstein space. 2008.
- [25] Alex Toth and Carl T Kelley. Convergence analysis for Anderson acceleration. *SIAM Journal on Numerical Analysis*, 53(2):805–819, 2015.
- [26] Fuchao Wei, Chenglong Bao, and Yang Liu. A class of short-term recurrence Anderson mixing methods and their applications. In *International Conference on Learning Representations*, 2022.
- [27] Ke Sun, Yafei Wang, Yi Liu, Bo Pan, Shangling Jui, Bei Jiang, Linglong Kong, et al. Damped anderson mixing for deep reinforcement learning: Acceleration, convergence, and stabilization. *Advances in Neural Information Processing Systems*, 34:3732–3743, 2021.
- [28] Hailiang Liu, Jia-Hao He, and Xuping Tian. Anderson acceleration of gradient methods with energy for optimization problems. *Communications on Applied Mathematics and Computation*, 6(2):1299–1318, 2024.
- [29] Anya Katsevich and Philippe Rigollet. On the approximation accuracy of gaussian variational inference. *The Annals of Statistics*, 52(4):1384–1409, 2024.
- [30] Michael Ziyang Diao, Krishna Balasubramanian, Sinho Chewi, and Adil Salim. Forward-backward gaussian variational inference via jko in the bures-wasserstein space. In *International Conference on Machine Learning*, pages 7960–7991. PMLR, 2023.
- [31] Viet Anh Nguyen, Soroosh Shafeezadeh-Abadeh, Daniel Kuhn, and Peyman Mohajerin Esfahani. Bridging bayesian and minimax mean square error estimation via wasserstein distributionally robust optimization. *Mathematics of Operations Research*, 48(1):1–37, 2023.
- [32] Lee Jaejin and Gyu Joo Han. Convergence analysis of fixed-point iteration with anderson acceleration on a simplified neutronics/thermal-hydraulics system. *Nuclear Engineering and Technology*, 54(2):532–545, 2022.
- [33] Sinho Chewi, Tyler Maunu, Philippe Rigollet, and Austin J Stromme. Gradient descent algorithms for Bures-Wasserstein barycenters. In *Conference on Learning Theory*, pages 1276–1304. PMLR, 2020.
- [34] Steven Diamond and Stephen Boyd. CVXPY: A Python-embedded modeling language for convex optimization. *Journal of Machine Learning Research*, 2016. To appear.
- [35] P-A Absil, Robert Mahony, and Rodolphe Sepulchre. Optimization algorithms on matrix manifolds. In *Optimization Algorithms on Matrix Manifolds*. Princeton University Press, 2009.
- [36] James Townsend, Niklas Koep, and Sebastian Weichwald. Pymanopt: A python toolbox for optimization on manifolds using automatic differentiation. *Journal of Machine Learning Research*, 17(137):1–5, 2016.
- [37] Jason Altschuler, Sinho Chewi, Patrik R Gerber, and Austin Stromme. Averaging on the Bures-Wasserstein manifold: dimension-free convergence of gradient descent. *Advances in Neural Information Processing Systems*, 34:22132–22145, 2021.
- [38] Martial Aguech and Guillaume Carlier. Barycenters in the Wasserstein space. *SIAM Journal on Mathematical Analysis*, 43(2):904–924, 2011.
- [39] Zoran Gajic and Muhammad Tahir Javed Qureshi. *Lyapunov matrix equation in system stability and control*. Courier Corporation, 2008.
- [40] Matyáš Novák, Jiří Vackář, Robert Cimrman, and Ondřej Šípr. Adaptive Anderson mixing for electronic structure calculations. *Computer Physics Communications*, 292:108865, 2023.
- [41] Bruce M Irons and Robert C Tuck. A version of the Aitken accelerator for computer iteration. *International Journal for Numerical Methods in Engineering*, 1(3):275–277, 1969.

A Omitted proofs

A.1 Properties of \mathcal{N}_0^d in a neighborhood of a distribution with a nondegenerate covariance matrix

In this section we collect technical lemmata on the local properties of the Bures-Wasserstein manifold. In particular, we relate the Bures-Wasserstein distance between the distributions and norms of the tangent vectors to Frobenius

norms of the matrices in $\text{Sym}(\mathbb{R}^d)$ that represent them. These lemmata are used to prove that the main assumptions on the manifold, needed for the local convergence of RAM, hold in a neighborhood of a nondegenerate fixed-point (c.f. Theorem 5). In the following sections, they will also be utilized in order to establish the contractivity of one of the operators in questions, as well as to analyze the properties of vector transport mappings.

The set \mathcal{N}_0^d of Gaussian distributions with mean zero and nondegenerate covariance matrix is not complete with respect to the Wasserstein distance. But since the Wasserstein distance metricizes weak convergence and it is equivalent to pointwise convergence of the characteristic functions, one can identify [22] the closure to the set

$$\overline{\mathcal{N}_0^d} = \left\{ \mu : \varphi_\mu(\xi) = e^{-\frac{1}{2}\xi^T \Sigma \xi}, \quad \Sigma^T = \Sigma \succeq 0 \right\}$$

where φ_μ denotes the characteristic function of μ .

Let us denote a Bures-Wasserstein ball with center Σ_* and radius r , as

$$B_r(\Sigma_*) := \{ \Sigma \in \mathcal{N}_0^d : W_2(\Sigma, \Sigma_*) \leq r \} \quad (42)$$

In the following, we show that the difference in the eigenvalues of the covariance matrices can be controlled by the Bures-Wasserstein distance between the respective distributions. Thus, the distributions in a small ball $B_r(\Sigma_*)$ around a nondegenerate distribution Σ_* have covariance matrices uniformly bound from above and bounded away from zero. This allows to prove several technical lemmas, useful for the analysis of the fixed-point operators and the RAM method.

Lemma 1. *Let $\rho_0, \rho_1 \in \overline{\mathcal{N}_0^d}$, with covariance matrices $\Sigma_0 \succ 0, \Sigma_1 \succeq 0$. If the Wasserstein distance $W_2^2(\rho_0, \rho_1) \leq r^2$, then the following bound on the eigenvalues $\lambda_1^1 \geq \dots \lambda_d^1$ of Σ_1 holds:*

$$\sum_k \left(\sqrt{\lambda_k^0} - \sqrt{\lambda_k^1} \right)^2 \leq r^2. \quad (43)$$

In particular,

$$\lambda_d^1 \geq \left(\sqrt{\lambda_d^0} - r \right)^2, \quad (44)$$

$$\lambda_1^1 \leq \left(\sqrt{\lambda_1^0} + r \right)^2. \quad (45)$$

Proof.

$$r^2 = W_2^2(\Sigma_0, \Sigma_1) = \text{Tr } \Sigma_0 + \text{Tr } \Sigma_1 - 2 \text{Tr } \tilde{\Sigma} = \sum_k \lambda_k^0 + \lambda_k^1 - 2\tilde{\lambda}_k$$

where $\tilde{\Sigma} = \left(\Sigma_0^{1/2} \Sigma_1 \Sigma_0^{1/2} \right)^{1/2}$ and $\tilde{\lambda}_k$ its eigenvalues. Since $\tilde{\Sigma}$ is symmetric, its eigenvalues and singular values correspond. Since $\tilde{\Sigma}^T \tilde{\Sigma} = \Sigma_0^{1/2} \Sigma_1 \Sigma_0^{1/2} = \left(\Sigma_1^{1/2} \Sigma_0^{1/2} \right)^T \Sigma_1^{1/2} \Sigma_0^{1/2}$, the singular values of $\tilde{\Sigma}$ are the same as the singular values of $\Sigma_1^{1/2} \Sigma_0^{1/2}$. As for the singular values of $\Sigma_1^{1/2} \Sigma_0^{1/2}$,

$$\sum_k \sigma_k \left(\Sigma_1^{1/2} \Sigma_0^{1/2} \right) \leq \sum_k \sigma_k \left(\Sigma_0^{1/2} \right) \sigma_k \left(\Sigma_1^{1/2} \right) = \sum_k \sqrt{\lambda_k^0 \lambda_k^1}.$$

Thus,

$$r^2 = \sum_k \lambda_k^0 + \lambda_k^1 - 2\tilde{\lambda}_k \geq \sum_k \lambda_k^0 + \lambda_k^1 - 2\sqrt{\lambda_k^0 \lambda_k^1} = \left(\sqrt{\lambda_k^0} - \sqrt{\lambda_k^1} \right)^2$$

and (44), (45) follow directly. \square

In the sequel we focus on a ball $B_r(\Sigma_*)$. We denote $0 < \lambda_1^* \leq \dots \leq \lambda_d^*$ the eigenvalues of Σ_* . The radius r is small enough such that $\sqrt{\lambda_1^*} - 2r > 0$.

The following lemma allows us to relate the norms of the vectors in the different tangent spaces:

Lemma 2. *If $\Sigma, \Sigma_1, \Sigma_2 \in B_r(\Sigma_*)$, $V \in \text{Tan}_{\Sigma_1} \mathcal{N}_0^d$, then the following estimates hold*

$$(\sqrt{\lambda_d^*} - r) \|V\|_F \leq \|V\|_\Sigma \leq (\sqrt{\lambda_1^*} + r) \|V\|_F \quad (46)$$

$$\|V\|_{\Sigma_2} \leq \frac{\sqrt{\lambda_1^*} + r}{\sqrt{\lambda_d^*} - r} \|V\|_{\Sigma_1} \quad (47)$$

Proof. Assuming $A \in \mathbb{R}^{d \times d}$, $B \in \text{Sym}(\mathbb{R}^d)$, $\lambda_1 \text{Id} \succeq B \succeq \lambda_d \text{Id}$

$$\begin{aligned}\text{Tr}(A^T B A) &= \sum_i a_i^T B a_i \geq \lambda_d \sum_i a_i^T a_i \geq \lambda_d \text{Tr}(A^T A) = \lambda_d \|A\|_F^2 \\ \text{Tr}(A^T B A) &= \sum_i a_i^T B a_i \leq \lambda_1 \sum_i a_i^T a_i \leq \lambda_1 \text{Tr}(A^T A) = \lambda_1 \|A\|_F^2\end{aligned}$$

where a_i are columns of A . For $\Sigma \in \mathcal{N}_0^d$, $V \in \text{Tan}_\Sigma \mathcal{N}_0^d$, plugging $A \leftarrow V$, $B \leftarrow \Sigma$

$$\lambda_d(\Sigma) \|V\|_F^2 \leq \|V\|_\Sigma^2 \leq \lambda_1(\Sigma) \|V\|_F^2 \quad (48)$$

Using the uniform bounds (44)-(45), one arrives at (46). Combining (46) twice for $\Sigma = \Sigma_{1,2}$, one gets (47). \square

Lemma 3. Let $\Sigma_1, \Sigma_2 \in B_r(\Sigma_*)$ with $r < \frac{1}{2}\sqrt{\lambda_d^*}$. Then the Frobenius norm between the covariance matrices can be controlled by the Bures-Wasserstein distance between the distributions, i.e.

$$\|\Sigma_1 - \Sigma_2\|_F \leq 2\sqrt{2} \left(\sqrt{\lambda_1^*} + \sqrt{\lambda_d^*} \right) W_2(\Sigma_1, \Sigma_2) \quad (49)$$

Proof. In the dynamic OT formulation

$$W_2^2(\Sigma_1, \Sigma_2) = \inf_{\Sigma(\cdot) \in \mathcal{A}} \frac{1}{2} \int \|V(t)\|_{\Sigma(t)}^2 dt \quad (50)$$

where $V(t) \in \text{Tan}_{\Sigma(t)} \mathcal{N}_0^d$ is a tangent vector to the curve $\Sigma(t)$, and the admissible set of curves \mathcal{A} is defined as

$$\mathcal{A} := \left\{ \Sigma(t) : t \in [0, 1] \left| \begin{array}{l} \Sigma(t) \in \mathcal{N}_0^d \\ \Sigma(0) = \Sigma_1 \\ \Sigma(1) = \Sigma_2 \end{array} \right. \right\} \quad (51)$$

First, we show that the infimum in (50) wouldn't change if we only consider such curves that $W_2(\Sigma(t), \Sigma_*) \leq 2r \forall t \in [0, 1]$. Since $\Sigma_1, \Sigma_2 \in B_r(\Sigma_*)$, from the triangle inequality we argue that

$$W_2(\Sigma_1, \Sigma_2) \leq W_2(\Sigma_1, \Sigma_*) + W_2(\Sigma_*, \Sigma_2) \leq 2r$$

Indeed, let us consider a curve $\Sigma(\cdot)$ and fix some $t \in [0, 1]$. We denote $\Sigma_t := \Sigma(t)$. The length of the curve is not smaller than the length of the piecewise geodesic:

$$L(\Sigma(\cdot)) := \sqrt{\frac{1}{2} \int \|V(t)\|_{\Sigma(t)}^2 dt} \geq W_2(\Sigma_1, \Sigma_t) + W_2(\Sigma_t, \Sigma_2)$$

Considering the triangle inequality for geodesic triangles $\Delta \Sigma_1 \Sigma_* \Sigma_t$ and $\Delta \Sigma_* \Sigma_t \Sigma_2$, one gets:

$$\begin{aligned}W_2(\Sigma_*, \Sigma_t) &\leq W_2(\Sigma_1, \Sigma_t) + W_2(\Sigma_*, \Sigma_1) \implies W_2(\Sigma_1, \Sigma_t) \geq W_2(\Sigma_*, \Sigma_t) - W_2(\Sigma_*, \Sigma_1) \\ W_2(\Sigma_*, \Sigma_t) &\leq W_2(\Sigma_t, \Sigma_2) + W_2(\Sigma_2, \Sigma_*) \implies W_2(\Sigma_t, \Sigma_2) \geq W_2(\Sigma_*, \Sigma_t) - W_2(\Sigma_*, \Sigma_2)\end{aligned}$$

Combining with the previous inequality one gets

$$L(\Sigma(\cdot)) \geq W_2(\Sigma_1, \Sigma_t) + W_2(\Sigma_t, \Sigma_2) \geq 2W_2(\Sigma_*, \Sigma_t) - W_2(\Sigma_*, \Sigma_2) - W_2(\Sigma_*, \Sigma_1) > 2W_2(\Sigma_t, \Sigma_*) - 2r$$

If the curve is such that $W_2(\Sigma_t, \Sigma_*) > 2r$, we argue that

$$L(\Sigma(\cdot)) > 4r - 2r = 2r \geq W_2(\Sigma_1, \Sigma_2)$$

and the curve is not optimal. Let's denote the improved admissible set of curves by

$$\mathcal{A}_r := \left\{ \Sigma(t) : t \in [0, 1] : \begin{array}{l} \Sigma(t) \in \mathcal{N}_0^d \\ W_2(\Sigma(t), \Sigma_*) \leq 2r \ \forall t \in [0, 1] \\ \Sigma(0) = \Sigma_1 \\ \Sigma(1) = \Sigma_2 \end{array} \right\} \quad (52)$$

$V(t)$ and $\dot{\Sigma}(t)$ are related as follows:

$$\Sigma(t + \tau) \underset{\tau \rightarrow 0}{\approx} (\text{Id} + \tau V(t)) \Sigma(t) (\text{Id} + \tau V(t))$$

thus

$$\dot{\Sigma}(t) = \Sigma(t) V(t) + V(t) \Sigma(t)$$

Let us define the operator P_Σ

$$P_\Sigma : (\text{Sym}(\mathbb{R}^d), \|\cdot\|_F) \rightarrow (\text{Sym}(\mathbb{R}^d), \|\cdot\|_F)$$

$$P_\Sigma[V] = \Sigma V + V\Sigma$$

For $U, V \in \text{Sym}(\mathbb{R}^d)$

$$\langle U, P_\Sigma[V] \rangle_F = \text{Tr}(U(\Sigma V + V\Sigma)) = 2\text{Tr}(U\Sigma V)$$

Thus, P_Σ is symmetric. On the admissible set of curves \mathcal{A}_r , the following bound on its spectrum can be made using (46):

$$2(\sqrt{\lambda_d^*} - 2r)^2 \|V\|_F^2 \leq \langle V, P_\Sigma[V] \rangle_F \leq 2(\sqrt{\lambda_1^*} + 2r)^2$$

Thus, P_Σ is invertible. We define $L_\Sigma := P_\Sigma^{-1}$. For L_Σ it holds

$$\langle U, L_\Sigma[U] \rangle_F \geq \frac{1}{2(\sqrt{\lambda_1^*} + 2r)^2} \|U\|_F^2 \quad (53)$$

For our curve $\Sigma(t)$, since $V(t)$ is tangent, we have

$$\dot{\Sigma}(t) = P_{\Sigma(t)}[V(t)]$$

$$V(t) = L_{\Sigma(t)}[\dot{\Sigma}(t)]$$

Then (omitting time dependence for brevity)

$$\begin{aligned} \|V\|_\Sigma^2 &= \text{Tr}(V\Sigma V) = \frac{1}{2} \text{Tr}(V(\Sigma V + V\Sigma)) = \frac{1}{2} \text{Tr}(V\dot{\Sigma}) = \\ &= \frac{1}{2} \text{Tr}(L_\Sigma[\dot{\Sigma}]\dot{\Sigma}) = \frac{1}{2} \langle \dot{\Sigma}, L_\Sigma[\dot{\Sigma}] \rangle_F \geq \frac{1}{2(\sqrt{\lambda_1^*} + 2r)^2} \|\dot{\Sigma}\|_F^2 \end{aligned}$$

where the final inequality holds only for the curves in \mathcal{A}_r .

Combining the estimates, we arrive at

$$\begin{aligned} W_2^2(\Sigma_1, \Sigma_2) &= \inf_{\mathcal{A}} \frac{1}{2} \int \|V(t)\|_{\Sigma(t)}^2 dt = \\ &= \inf_{\mathcal{A}_r} \frac{1}{2} \int \|V(t)\|_{\Sigma(t)}^2 dt = \inf_{\mathcal{A}_r} \frac{1}{4} \int \text{Tr}(L_{\Sigma(t)}[\dot{\Sigma}(t)]\dot{\Sigma}(t)) dt \geq \\ &\stackrel{(*)}{\geq} \frac{1}{8(\sqrt{\lambda_1^*} + \sqrt{\lambda_d^*})^2} \inf_{\substack{\Sigma(t) \in \mathcal{N}_0^d \\ \Sigma(0) = \Sigma_1 \\ \Sigma(1) = \Sigma_2}} \int \|\dot{\Sigma}(t)\|_F^2 dt = \frac{\|\Sigma_1 - \Sigma_2\|_F^2}{8(\sqrt{\lambda_1^*} + \sqrt{\lambda_d^*})^2} \end{aligned}$$

In (*), we can minimize with respect to the original admissible set \mathcal{A} , since $\mathcal{A}_r \subset \mathcal{A}$ and thus $\inf_{\mathcal{A}} \mathcal{F} \leq \inf_{\mathcal{A}_r} \mathcal{L}$ for any functional \mathcal{L} .

$$\Sigma_e(t) := (1-t)\Sigma_1 + t\Sigma_2$$

and $\sqrt{\lambda_d^*} < 2r$. Thus

$$\|\Sigma_1 - \Sigma_2\|_F \leq 2\sqrt{2}(\sqrt{\lambda_1^*} + \sqrt{\lambda_d^*})W_2(\Sigma_1, \Sigma_2)$$

□

The explicit expression for the sectional curvature of the Bures-Wasserstein space is given in [21, Theorem 1.1]. Its minimal and maximal values depend only on the minimal and maximal eigenvalues of the covariance matrix. We express this fact the following corollary

Corollary 1. *For every $\Sigma \in B_r(\Sigma_*)$, the sectional curvature K_Σ of \mathcal{N}_0^d at Σ can uniformly bound by*

$$0 \leq K_\Sigma(e_1, e_2) \leq \frac{3(\sqrt{\lambda_1^*} + r)^4}{2(\sqrt{\lambda_d^*} - r)^6}. \quad (54)$$

where e_1, e_2 are the directions, defining the plane and $r < \sqrt{\lambda_d^*}$

We can finally formulate the theorem showing that the main assumptions of the RAM's convergence hold for $B_r(\Sigma_*)$ (analogous to Assumption 1 of [14]).

Theorem 5. Let Σ_* be a nondegenerate covariance matrix and $r < \frac{2}{3}\sqrt{\lambda_d^*}$. The ball $B_r(\Sigma_*)$ is compact in \mathcal{N}_0^d with bounded sectional curvature. For every $V \in \text{Tan}_\Sigma \mathcal{N}_0^d$ such that $\|V\|_\Sigma \leq \frac{1}{2}r$, it holds that $W_2(\Sigma, \text{Exp}_\Sigma(V)) = \|V\|_\Sigma$ for all $\Sigma \in \mathcal{M}$.

Proof of Theorem 5. Closedness of the ball and the sectional curvature bounds are due to Lemma 1 and Corollary 1.

Every tangent vector V induces a mapping $T(x) = Vx + x = (\text{Id} + V)x = \nabla_x \frac{1}{2}\langle x, (\text{Id} + V)\rangle$. Using (46), we get

$$\|V\|_o \leq \|V\|_F \leq \frac{1}{\sqrt{\lambda_*^d} - r} \|V\|_\Sigma \leq \frac{r}{2(\sqrt{\lambda_*^d} - r)} = \frac{2/3}{2(1 - 2/3)} = 1$$

Since $\|V\|_o \leq 1$, operator $(\text{Id} + V)$ has nonnegative eigenvalues, and the mapping T is a gradient of a convex function. Thus, the mapping is optimal, and its L_2 norm is equal to the Wasserstein distance between the distributions. \square

A.2 Contraction coefficients of the operators

For the operators of the form

$$G(\rho) = \text{Exp}_\rho(-h\partial_W \mathcal{E}(\rho)) \quad (55)$$

the contraction estimate can be deduced as follows. Consider random variables $x' \sim G(\rho_1)$, $y' \sim G(\rho_2)$, and a coupling

$$\begin{aligned} x' &= x - h\partial_W \mathcal{E}(\rho_1, x) \\ y' &= y - h\partial_W \mathcal{E}(\rho_2, y) \\ (x, y) &\sim \gamma_{\text{opt}} \end{aligned}$$

where γ_{opt} is an optimal plan between ρ_1 and ρ_2 . This coupling is a valid coupling between $G(\rho_1)$ and $G(\rho_2)$. Thus

$$\begin{aligned} W_2^2(G(\rho_1), G(\rho_2)) &\leq \int \|x' - y'\|_2^2 d\gamma_{\text{opt}} = \int \|x - y - h(\partial_W \mathcal{E}(\rho_1, x) - \partial_W \mathcal{E}(\rho_2, y))\|_2^2 d\gamma_{\text{opt}} = \\ &= \int \|x - y\|_2^2 d\gamma_{\text{opt}} - 2h \int \langle \partial_W \mathcal{E}(\rho_1, x) - \partial_W \mathcal{E}(\rho_2, y), x - y \rangle d\gamma_{\text{opt}} + h^2 \int \|\partial_W \mathcal{E}(\rho_1, x) - \partial_W \mathcal{E}(\rho_2, y)\|_2^2 d\gamma_{\text{opt}} \end{aligned} \quad (56)$$

If the functional \mathcal{E} is λ -convex a.g.g., then the second term can be estimated as follows [1, Equation 10.1.8]:

$$\int \langle \partial_W \mathcal{E}(\rho_1, x) - \partial_W \mathcal{E}(\rho_2, y), x - y \rangle d\gamma_{\text{opt}} \geq \frac{1}{2}\lambda W_2^2(\rho_1, \rho_2) \quad (57)$$

To estimate the final term, we can define the generalization of the Lipschitz gradient property in the following way.

Definition A.1. A functional $\mathcal{E} : \mathcal{P}_2(\mathbb{R}^d) \rightarrow \mathbb{R}$ has L -Lipschitz Wasserstein gradient for some subset $\mathcal{S} \subseteq \mathcal{P}_2(\mathbb{R}^d)$, if its Wasserstein gradient

$$\partial_W \mathcal{E}(\rho) = \nabla \frac{\delta \mathcal{E}}{\delta \rho} \in L_2(\rho) \quad \forall \rho \in \mathcal{S}$$

and there exists a constant $L > 0$ such that $\forall \rho_1, \rho_2 \in \mathcal{S}$

$$\int \|\partial_W \mathcal{E}(\rho_1, x) - \partial_W \mathcal{E}(\rho_2, y)\|_2^2 d\gamma_{\text{opt}} \leq L^2 W_2^2(\rho_1, \rho_2) \quad (58)$$

Proposition A.1. If the functional \mathcal{E} is λ -convex along generalized geodesics and has L -Lipschitz Wasserstein gradient, then the operator $\text{Exp}_\rho(-h\partial_W \mathcal{E})$ is contractive for small enough h .

Proof. Plugging (57) and (58) into (56), one gets

$$W_2^2(G(\rho_1), G(\rho_2)) \leq (1 - \lambda h + h^2 L^2) W_2^2(\rho_1, \rho_2)$$

The coefficient in front of $W_2^2(\rho_1, \rho_2)$ is smaller than one if $h \in (0, \frac{\lambda}{L^2})$. In particular, the optimal step is $h = \frac{\lambda}{2L^2}$. \square

In [1], there are multiple examples of λ -convex a.g.g. functionals. In particular, for the functional $\mathcal{E} = \text{KL}(\cdot | \rho_\infty)$, where $\rho_\infty = e^{-V}$, \mathcal{E} is λ -convex when V is λ -convex. The Lipschitz gradient property, up to the authors' best knowledge, hasn't been thoroughly studied before. In the following, we perform this analysis in the case of the $\text{KL}(\cdot | \rho_\infty)$ functional, constrained to the Bures-Wasserstein manifold. Let's compute in case of Gaussians, $\rho_i = \mathcal{N}(0, \Sigma_i)$, $i = 1, 2$.

Lemma 4. Let Σ_* be a nondegenerate covariance matrix. The functional

$$\text{KL}(\cdot | \Sigma_*) : \mathcal{N}_0^d \rightarrow \mathbb{R}^d$$

has L -Lipschitz Wasserstein gradient on a ball $B_r(\Sigma_*)$ where

$$r < \frac{1}{16\sqrt{2} \left(1 + \sqrt{\frac{\lambda_1^*}{\lambda_d^*}}\right)} \sqrt{\lambda_d^*} \quad (59)$$

and

$$L^2 = \frac{4}{(\sqrt{\lambda_d^*} - r)^4} \left(1 + 4 \frac{(\sqrt{\lambda_1^*} + 2r)^4}{(\sqrt{\lambda_d^*} - r)^4} \right)$$

Proof. The idea of the proof is to work with the explicit form of (56) and split the quantity under the integral w.r.t. $d\gamma_{\text{opt}}$ in two parts. The first is “linear part” in form of $\|A(x - y)\|$ for some operator A , which can be directly related to the Bures-Wasserstein distance. The second term is a “nonlinear part” $\|\Sigma_1^{-1} - \Sigma_2^{-1}\|_F$, which we treat by first considering the linearization w.r.t. $\|\Sigma_1 - \Sigma_2\|_F$, and then relating the norm difference to the Wasserstein distance using (18).

Assuming that $\Sigma_1, \Sigma_2 \in B_r$ with $r < \frac{1}{2}\sqrt{\lambda_d^*}$, so that the previous lemmata can be used, we proceed with the calculation:

$$\begin{aligned} & \int \|\partial_W \mathcal{E}(\Sigma_1, x) - \partial_W \mathcal{E}(\Sigma_2, y)\|^2 d\gamma_{\text{opt}} = \\ &= \int \|(\Sigma_1^{-1} - \Sigma_*^{-1})x - (\Sigma_2^{-1} - \Sigma_*^{-1})y\|^2 d\gamma_{\text{opt}} = \int \|(\Sigma_1^{-1} - \Sigma_*^{-1})(x - y) + (\Sigma_1^{-1} - \Sigma_2^{-1})y\|^2 d\gamma_{\text{opt}} \leq \\ &\leq 2\|\Sigma_1^{-1} - \Sigma_*^{-1}\|_o^2 \int \|x - y\|^2 d\gamma_{\text{opt}} + 2 \int \|(\Sigma_1^{-1} - \Sigma_2^{-1})y\|^2 d\gamma_{\text{opt}} = \\ &= 2\|\Sigma_1^{-1} - \Sigma_*^{-1}\|_o^2 W_2^2(\Sigma_1, \Sigma_2) + 2 \left\| \Sigma_2^{1/2}(\Sigma_1^{-1} - \Sigma_2^{-1}) \right\|_F^2 \leq \\ &\leq 2\|\Sigma_1^{-1} - \Sigma_*^{-1}\|_o^2 W_2^2(\Sigma_1, \Sigma_2) + 2\|\Sigma_2\|_o \|\Sigma_1^{-1} - \Sigma_2^{-1}\|_F^2 \quad (60) \end{aligned}$$

where $\|\cdot\|_o$ and $\|\cdot\|_F$ stand for operator and Frobenius norm, respectively.

Considering the quantity $\|\Sigma_1^{-1} - \Sigma_2^{-1}\|_F$ as $\|\Sigma_1 - \Sigma_2\|_F \rightarrow 0$.

$$\begin{aligned} \Sigma_2^{-1} &= [\Sigma_1 - (\Sigma_1 - \Sigma_2)]^{-1} = \Sigma_1^{-1} \left[\text{Id} - \underbrace{(\Sigma_1 - \Sigma_2)\Sigma_1^{-1}}_{:= \Delta \Sigma} \right]^{-1} = \\ &= \Sigma_1^{-1} [\text{Id} + \Delta \Sigma + \Delta \Sigma^2 + \dots] = \Sigma_1^{-1} [\text{Id} + \Delta \Sigma + R] \end{aligned}$$

In order to bound the remainder of the series R , Σ_1 and Σ_2 should be sufficiently close. Let us find the exact condition before we proceed. Since Σ_1, Σ_2 are both symmetric

$$\begin{aligned} \|\Delta \Sigma\|_F^2 &= \|(\Sigma_1 - \Sigma_2)\Sigma_1^{-1}\|_F^2 = \\ &= \text{Tr}(\Sigma_1^{-1}(\Sigma_1 - \Sigma_2)^2 \Sigma_1^{-1}) = \text{Tr}((\Sigma_1^{-1}(\Sigma_1 - \Sigma_2))^T (\Sigma_1^{-1}(\Sigma_1 - \Sigma_2))) = \\ &= \|\Sigma_1^{-1}(\Sigma_1 - \Sigma_2)\|_F^2 \end{aligned}$$

where symmetry of the matrices and the cyclic property of the trace was used. Using (43) and (18)

$$\begin{aligned} \|\Delta \Sigma\|_F &= \|\Sigma_1^{-1}(\Sigma_1 - \Sigma_2)\|_F \leq \\ &\leq \|\Sigma_1^{-1}\|_o \|\Sigma_1 - \Sigma_2\|_F \leq \frac{2\sqrt{2}(\sqrt{\lambda_1^*} + 2r)}{(\sqrt{\lambda_d^*} - r)^2} W_2(\Sigma_1, \Sigma_2) \leq \\ &\leq \frac{8\sqrt{2}(\sqrt{\lambda_1^*} + \sqrt{\lambda_d^*})}{\lambda_d^*} W_2(\Sigma_1, \Sigma_2) \end{aligned}$$

since r has to be less than $\frac{1}{2}\sqrt{\lambda_d^*}$. Thus, if

$$W_2(\Sigma_1, \Sigma_2) \leq \frac{1}{16\sqrt{2}\left(1 + \sqrt{\frac{\lambda_1^*}{\lambda_d^*}}\right)}\sqrt{\lambda_d^*} \implies \|\Delta\Sigma\|_F \leq \frac{1}{2}$$

If $\|\Delta\Sigma\| \leq \frac{1}{2}$, the remainder of the series R can be estimated as

$$\begin{aligned} \|R\|_F &= \|\Delta\Sigma^2 + \Delta\Sigma^3 + \dots\|_F \leq \|\Delta\Sigma\|_F^2 + \|\Delta\Sigma\|_F^3 + \dots = \\ &= \|\Delta\Sigma\|_F^2 (1 + \|\Delta\Sigma\|_F + \|\Delta\Sigma\|_F^2 + \dots) = \frac{\|\Delta\Sigma\|_F^2}{1 - \|\Delta\Sigma\|_F} \leq 2\|\Delta\Sigma\|_F^2 \end{aligned}$$

Thus, we constrain the radius of the ball r to be

$$r \leq \frac{1}{16\sqrt{2}\left(1 + \sqrt{\frac{\lambda_1^*}{\lambda_d^*}}\right)}\sqrt{\lambda_d^*} \leq \frac{1}{32\sqrt{2}}\sqrt{\lambda_d^*}$$

Since $\frac{1}{32\sqrt{2}} < \frac{1}{2}$, the usage of (18) was justified. Using this relation, we can get

$$\begin{aligned} \|\Sigma_1^{-1} - \Sigma_2^{-1}\|_F^2 &= \|\Sigma_1^{-1}(\Sigma_1 - \Sigma_2)\Sigma_1^{-1} + \Sigma_1^{-1}R\|_F^2 \leq \\ &\leq \|\Sigma_1^{-1}\|_o^2\|\Delta\Sigma + R\|_F^2 \leq 2\|\Sigma_1^{-1}\|_o^2(\|\Delta\Sigma\|_F^2 + \|R\|_F^2) \leq \\ &\leq 2\|\Sigma_1^{-1}\|_o^2(\|\Delta\Sigma\|_F^2 + 4\|\Delta\Sigma\|_F^4) \leq 4\|\Sigma_1^{-1}\|_o^2\|\Delta\Sigma\|_F^2 \quad (61) \end{aligned}$$

Thus

$$\|\Sigma_1^{-1} - \Sigma_2^{-1}\|_F^2 \leq \|\Sigma_1^{-1}\|_o^4\|\Sigma_1 - \Sigma_2\|_F^2 \leq \frac{8(\sqrt{\lambda_1^*} + 2r)^2}{(\sqrt{\lambda_d^*} - r)^8}W_2^2(\Sigma_1, \Sigma_2)$$

We can finish the bound in (60)

$$\begin{aligned} \int \|\partial_W \mathcal{E}(\Sigma_1, x) - \partial_W \mathcal{E}(\Sigma_2, y)\|^2 d\gamma_{\text{opt}} &\leq \\ &\leq \left(2\|\Sigma_1^{-1} - \Sigma_2^{-1}\|_o^2 + 2\|\Sigma_2\|_o \frac{8(\sqrt{\lambda_1^*} + 2r)^2}{(\sqrt{\lambda_d^*} - r)^8}\right)W_2^2(\Sigma_1, \Sigma_2) \leq \\ &\leq \frac{4}{(\sqrt{\lambda_d^*} - r)^4} \left(1 + 4 \frac{(\sqrt{\lambda_1^*} + 2r)^4}{(\sqrt{\lambda_d^*} - r)^4}\right)W_2^2(\Sigma_1, \Sigma_2) \quad (62) \end{aligned}$$

□

A.3 Derivation of Proposition 3.1

Proof. We extend scalar product (13) to the whole $\mathbb{R}^{d \times d}$ as $\langle U, V \rangle_\Sigma := \text{Tr}(U^T \Sigma V)$ and pose the projection as the constrained minimization problem:

$$\Pi_\Sigma(V) = \arg \min_X \|X - V\|_\Sigma^2 \quad (63)$$

$$\text{s.t. } X = X^T. \quad (64)$$

Writing out the Lagrangian and setting its derivatives to zero, one gets

$$\begin{aligned} L(X, \lambda) &= \text{Tr}((X - V)^T \Sigma (X - V)) + \langle \lambda, X - X^T \rangle_F, \\ \frac{\partial L}{\partial X} &= 0 \Rightarrow 2\Sigma X - 2\Sigma V = \lambda^T - \lambda, \\ \frac{\partial L}{\partial \lambda} &= 0 \Rightarrow X = X^T. \end{aligned}$$

Averaging the first equation and its transpose, with $X = X^T$, gives

$$\Sigma X + X\Sigma = \Sigma V + V^T \Sigma,$$

and setting $V = UT_{01}^{-1}$ yields Equation 23. The unique solution exists if the eigenvalues of Σ do not add up to zero:

$$\lambda_i + \lambda_j > 0 \quad \forall (i, j),$$

which always holds in our case since all the eigenvalues are positive. See also [39] for the overview of the numerical approaches. □

A.4 Proof of Theorem 3

Lemma 5 (cf. Lemma 8 in [14]). *Let $x_1, \dots, x_k \in \mathcal{B}_{\mathcal{N}_0^d}(\Sigma_*, \frac{1}{2}r_{\Sigma_*})$. Then there is M_1 such that*

$$\|X_k \Gamma_k\| + \|r_k\| \leq M_1 \sum_{j=0}^k \|r_{k-j}\|.$$

Proof. We observe that

$$\|\text{Exp}_{x_\ell}^{-1}(x_{\ell+1})\| = W_2(x_\ell, x_{\ell+1})$$

by optimality of Exp^{-1} . Then by the Lipschitz assumption in Assumption 4.1, we have

$$\begin{aligned} \|\Delta x_{k-j}^{(k)}\| &= \|\mathcal{T}_{x_{k-1}}^{x_k} \cdots \mathcal{T}_{x_{k-j}}^{x_{k-j+1}} \text{Exp}_{x_{k-j}}^{-1}(x_{k-j+1})\| \\ &\leq M^j \|\text{Exp}_{x_{k-j}}^{-1}(x_{k-j+1})\| \\ &= M^j W_2(x_{k-j}, x_{k-j+1}) \\ &\leq \frac{M^j}{L_1} \|r_{k-j+1} - \mathcal{P}_{x_{k-j}}^{x_{k-j+1}} r_{k-j}\|. \end{aligned}$$

It holds

$$\begin{aligned} \left\| \sum_{j=1}^i \Delta x_{k-j}^{(k)} \right\| &\leq \sum_{k=1}^i \|\Delta x_{k-j}^{(k)}\| \leq \sum_{j=1}^i \frac{M^j}{L_1} (\|r_{k-j+1}\| + \|r_{k-1}\|) \\ &\leq \frac{M}{L_1} \|r_k\| + \sum_{j=2}^i \frac{M^{j-1}(M+1)}{L_1} \|r_{k-j+1}\| + \frac{M^i}{L_1} \|r_{k-i}\|. \end{aligned}$$

Observe $2 \frac{\max\{M^m, M\}}{L_1} \geq \frac{1}{L_1} \max\{M^m + M^{m-1}, M^2 + M\}$. By Assumption 4.3 we have $\|\Gamma_k\| \leq M_\Gamma$. Hence,

$$\begin{aligned} \|X_k \Gamma_k\| + \|r_k\| &\leq \|\Gamma_k\| \sum_{j=1}^k \|\Delta x_{k-j}^{(k)}\| + \|r_k\| \\ &\leq 2M_\Gamma \frac{\max\{M^m, M\}}{L_1} (\|r_k\| + \sum_{j=2}^k \|r_{k-j+1}\| + \|r_0\|) + \|r_k\| \\ &\leq (2M_\Gamma \frac{\max\{M^m, M\}}{L_1} + 1) \sum_{j=0}^k \|r_{k-j}\|. \end{aligned}$$

□

Lemma 6 (cf. Proposition 2 in [14]). *Let $x_1, \dots, x_k \in \mathcal{B}_{\mathcal{N}_0^d}(\Sigma_*, \frac{r_{\Sigma_*}}{L_2(mM_1+\beta+1)})$. Let $z_k^i = \sum_{j=1}^i \Delta x_{k-j}^{(k)}$ and $y_k^i = \text{Exp}_{x_k}(-z_k^i)$. Then there is $M_2, M_3 > 0$ such that*

$$\|\mathcal{P}_{y_k^i}^{x_k} F(y_k^i) - \mathcal{T}_{x_{k-1}}^{x_k} \mathcal{T}_{x_{k-2}}^{x_{k-1}} \cdots \mathcal{T}_{x_{k-i}}^{x_{k-i+1}} F(x_{k-i})\| \leq M_2 \sum_{j=0}^i \|r_{k-j}\|^2.$$

Furthermore, for $w_k^i = \sum_{j=0}^i \gamma_j^k \Delta x_{k-j}^{(k)}$ and $v_k^i = \text{Exp}_{x_k}(-w_k^i)$ it holds

$$\|\mathcal{P}_{v_k^i}^{x_k} F(v_k^i) - \mathcal{P}_{v_{k-1}^i}^{x_k} F(v_{k-1}^{i-1}) - \gamma_i^k (\mathcal{P}_{y_k^i}^{x_k} F(y_k^i) - \mathcal{P}_{y_{k-1}^i}^{x_k} F(y_{k-1}^{i-1}))\| \leq M_3 \sum_{j=0}^i \|r_{k-j}\|^2.$$

Now let us prove Theorem 3

Proof. First we assume there are some $x_1, \dots, x_k \in \mathcal{B}_{\mathcal{N}_0^d}(\Sigma_*, \tilde{r})$ with $\tilde{r} < \frac{r_{\Sigma_*}}{2L_2(mM_1 + \beta + 1)}$. Define

$$\begin{cases} \bar{x}_k = \text{Exp}_{x_k}(-X_k \Gamma_k) \\ x_{k+1} = \text{Exp}_{x_k}(-X_k \Gamma_k + \beta_k \bar{r}_k) \\ \tilde{x}_{k+1} = \text{Exp}_{x_k}(-X_k \Gamma_k + \bar{r}_k) \end{cases}$$

with $\bar{r}_k = r_k - R_k \Gamma_r$. Then $\|\bar{r}_k\| \leq \|r_k\|$.

We observe

$$\begin{aligned} \|F(x_{k+1})\| &\leq L_2 W_2(x_{k+1}, x_*) \\ &\leq L_2(W_2(x_{k+1}, x_k) + W_2(x_k, x_*)) \\ &\leq L_2(W_2(x_{k+1}, x_k) + \tilde{r}) \\ &\leq L_2(\|X_k \Gamma_k + \beta \bar{r}_k\| + \tilde{r}) \\ &\leq L_2(M_1 \left(\sum_{i=0}^{\min\{k, m\}} \|r_{k-i}\| + \beta \|r_k\| \right) + \tilde{r}) \\ &\leq L_2(M_1 m \tilde{r} + \beta \tilde{r} + \tilde{r}) \\ &\leq L_2(M_1 m + \beta + 1) \tilde{r} \leq r_{\Sigma_*} \end{aligned}$$

Similarly, $W_2(\bar{x}_k, x^*), W_2(\tilde{x}_k, x^*) \leq L_2(M_1 m + \beta + 1) \tilde{r}$.

Hence, with Lemma 5 we get

$$\begin{aligned} \|r_{k+1}\| &= W_2(G(x_{k+1}), x_{k+1}) \\ &\leq W_2(G(x_{k+1}), G(\bar{x}_k)) + W_2(G(\bar{x}_k), x_{k+1}). \end{aligned}$$

By assumption,

$$W_2(G(x_{k+1}), G(\bar{x}_k)) \leq \kappa W_2(\text{Exp}_{x_k}(X_k \Gamma_k), \text{Exp}_{x_k}(X_k \Gamma_k + \beta_k \bar{r}_k)) \leq \kappa \|\beta_k \bar{r}_k\|.$$

Now

$$W_2(x_{k+1}, G(\bar{x}_k)) \leq W_2(G(\bar{x}_k), \tilde{x}_{k+1}) + W_2(\tilde{x}_{k+1}, x_{k+1}).$$

By assumption

$$W_2(\tilde{x}_{k+1}, x_{k+1}) \leq \|X_k \Gamma_k - \beta_k \bar{r}_k - X_k \Gamma_k + \bar{r}_k\| = (1 - \beta_k) \|\bar{r}_k\|.$$

Also

$$W_2(G(\bar{x}_k), \tilde{x}_{k+1}) \leq W_2(G(\bar{x}_k), \text{Exp}_{\bar{x}_k}(\mathcal{T}_{x_k}^{\bar{x}_k} \bar{r}_k)) + W_2(\text{Exp}_{\bar{x}_k}(\mathcal{T}_{x_k}^{\bar{x}_k} \bar{r}_k), \tilde{x}_{k+1}).$$

By Lemma 5 in [14] there is a constant c_0 depending on the sectional curvature such that

$$W_2(\text{Exp}_{\bar{x}_k}(\mathcal{T}_{x_k}^{\bar{x}_k} \bar{r}_k), \tilde{x}_{k+1}) \leq c_0 \underbrace{\min\{\|X_k \Gamma_k\|, \|\bar{r}_k\|\}}_{\leq \tilde{r}} (\|X_k \Gamma_k\| + \|\bar{r}_k\|)^2.$$

With Lemma 5 we get

$$(\|X_k \Gamma_k\| + \|\bar{r}_k\|)^2 \leq mM_1^2 \sum_{j=0}^k \|r_{k-j}\|^2.$$

Furthermore,

$$W_2(G(\bar{x}_k), \text{Exp}_{\bar{x}_k}(\mathcal{T}_{x_k}^{\bar{x}_k} \bar{r}_k)) = W_2(\text{Exp}_{\bar{x}_k}(-F(\bar{r}_k)), \text{Exp}_{\bar{x}_k}(\mathcal{T}_{x_k}^{\bar{x}_k} \bar{r}_k)) \leq \| -F(\bar{x}_k) - \mathcal{T}_{x_k}^{\bar{x}_k} \bar{r}_k \|.$$

Defining $w_k^i = \sum_{j=0}^i \gamma_j^k \Delta x_{k-j}^{(k)}$, $z_j^k = \sum_{j=0}^i \Delta x_{k-j}^{(k)}$, $v_k^i = \text{Exp}_{x_k}(-w_k^i)$ and $y_k^i = \text{Exp}_{x_k}(-z_k^i)$ we get by Lemma 6

$$\begin{aligned}
\| -F(\bar{x}_k) - \mathcal{T}_{x_k}^{\bar{x}_k} \bar{r}_k \| &= \|\mathcal{T}_{\bar{x}_k}^{x_k} F(\bar{x}_k) + \bar{r}_k\| \\
&= \|\mathcal{T}_{\bar{x}_k}^{x_k} F(\bar{x}_k) - F(x_k) - \sum_{i=1}^k \gamma_i^k \Delta r_{k-i}\| \\
&\leq \underbrace{\|\mathcal{P}_{v_k^i}^{x_k} F(v_k^i) - \mathcal{P}_{v_k^{i-1}}^{x_k} F(v_k^{i-1}) - \gamma_i^k (\mathcal{P}_{y_k^i}^{x_k} F(y_k^i) - \mathcal{P}_{y_k^{i-1}}^{x_k} F(y_k^{i-1}))\|}_{\leq M_3 \sum_{j=0}^i \|r_{k-j}\|^2} \\
&\quad + \underbrace{\sum_{i=1}^k |\gamma_i^k| \| -\Delta r_{k-i} + \mathcal{P}_{y_k^i}^{x_k} F(y_k^i) - \mathcal{P}_{y_k^{i-1}}^{x_k} F(y_k^{i-1})\|}_{\leq M_\Gamma (\|\mathcal{T}_{x_{k-1}}^{x_k} \cdots \mathcal{T}_{x_{k-i+1}}^{x_{k-i+2}} r_{k-i+1} + \mathcal{P}_{y_k^{i-1}}^{x_k} F(y_k^{i-1})\| + \|\mathcal{T}_{x_{k-1}}^{x_k} \cdots \mathcal{T}_{x_{k-i}}^{x_{k-i+1}} r_{k-i} + \mathcal{P}_{y_k^i}^{x_k} F(y_k^i)\|)} \\
&\leq (M_3 + 2M_\Gamma M_2) \sum_{i=0}^k \|r_{k-i}\|^2.
\end{aligned}$$

All-together, we get

$$\|r_{k+1}\| \leq (1 - \beta_k + \kappa \beta_k) \|\bar{r}_k\| + (c_0 \tilde{r} m M_1^2 + M_3 + 2M_\Gamma M_2) \sum_{i=0}^k \|r_{k-i}\|^2.$$

Now we want to show that the history produced by the algorithm fulfills these arguments. To that end we use induction. Define $\hat{r} = \min\{\frac{r_{\Sigma_*}}{L_2(mM_1+\beta+1)}, \frac{L_1-L_2+(1-\kappa)\beta L_2}{MmL_2^2}\}$. If $W_2(x_0, x_*) < \frac{\hat{r}}{1+L_2}$ we get

$$\|F(x_0)\| \leq L_2 W_2(x_0, x_*) \leq \frac{L_2}{1+L_2} \hat{r}$$

and

$$\begin{aligned}
W_2(x_1, x_*) &\leq W_2(x_1, x_0) + W_2(x_0, x_*) \\
&\leq \underbrace{\|\text{Exp}_{x_0}^{-1}(x_1)\|}_{=\|r_0\|} + \frac{1}{1+L_2} \hat{r} \\
&\leq \hat{r}.
\end{aligned}$$

Assume now that the assumption of the theorem is true for all $j \leq k$. Then by above considerations we have

$$\begin{aligned}
\|r_{k+1}\| &\leq (1 - \beta_k + \kappa \beta_k) \|r_k\| + M \sum_{j=0}^k \|r_{k-j}\|^2 \\
&\leq (1 - \beta_k + \kappa \beta_k) L_2 \hat{r} + MmL_2^2 \hat{r}^2 \\
&\leq L_1 \hat{r}.
\end{aligned}$$

Then we have

$$W_2(x_{k+1}, x_*) \leq \frac{1}{L_1} \|r_{k+1}\| \leq \hat{r}$$

and the claim follows by induction. \square

B Additional numeric results

For all the mentioned problems, a comprehensive set of numerical experiments has been conducted. We study the performance of the method depending on both the problem settings and the hyperparameters of the numeric solver. The selection of the former will be described for each problem individually. As for the method hyperparameters, for the BWRAM method we vary the relaxation parameter β_k , the maximal number of history vectors m , and the regularization

parameter $l_{\infty, \max}$. The number of historic vectors varies in the range from 1 to 15. In the current work, these are constant during the iterations. In principle, adaptive strategies for restarting the iteration [40, 15] or selection of the relaxation parameter [41], but these strategies are outside of the scope of the current work.

For the Ornstein-Uhlenbeck process and KL minimization, we consider multiple invariant distributions with covariance matrix being i.i.d realizations of the following random variable:

$$\Sigma_* = Q^T D Q, \quad D = \text{diag} \left(\sigma_{\min} + \frac{i-1}{d-1} (\sigma_{\max} - \sigma_{\min}) \right), \quad Q \text{ i.i.d. random orthogonal matrix.}$$

We fix σ_{\min} and vary d and σ_{\max} . For each pair of d , σ_{\max} , we run the Picard iteration and Anderson acceleration with different lengths of history m . The acceleration measured as $\frac{N_{\text{Picard}}}{N_{\text{AA}}}$ is averaged over several independent realizations of Q .

For the Ornstein-Uhlenbeck problem, the relaxation parameter and regularization parameter are set to be $\beta = 1.0$ and $l_{\infty, \max} = 1.0$. In Table 1a, one can see the maximal mean acceleration (averaged over 6 independent runs) of BWRAM, compared to Picard.

For the KL minimization problem, where the operator takes form

$$G(\Sigma) = \text{Exp}_{\Sigma}(-h \partial_W \text{KL}(\Sigma | \Sigma_*)),$$

the scaling parameter is set to $h = 0.3$, and the values of d , σ_{\min} , σ_{\max} are the same as in the Ornstein-Uhlenbeck problem. As for the hyperparameters of BWRAM, the regularization parameter takes values $l_{\text{inf}, \max} \in \{1.5, 10.0\}$. In case of fixed-point problems, with an operator defined by the Wasserstein gradient of some functional \mathcal{E} as $\text{Exp}(-h \partial_W \mathcal{E})$, the optimal stepsize parameter h may have different values for the basic Picard method and for RAM. One can compensate for that by choosing the relaxation β_k factor smaller or larger than one. We demonstrate it by varying the relaxation factor in the KL problem in the set $\beta \in \{0.9, 1.0, 1.2\}$. Maximal acceleration is achieved for $\beta = 1.2$ in most cases.

We also compare our method to established methods of Riemannian optimization. In particular, we consider Riemannian gradient descent (RGD) with backtracking line search, and Riemannian conjugate gradient descent, provided by the `pymanopt` [36] package. The results of the experiments are presented in Table 3. Here, the number of iterations is first averaged over $n = 6$ runs for random Σ_* , and then the minimal one is chosen among different values of the hyperparameters. The best result for each problem is marked bold.

Table 3: The mean number of steps for the KL minimization problem for each method.

d	σ_{\max}	Picard	RGD	BWRAM	RCG
4	5.0	45.0	53.0	11.0	25.0
	10.0	95.0	113.0	15.0	42.0
	20.0	196.0	162.0	18.2	56.0
8	5.0	45.0	39.0	14.0	33.0
	10.0	96.0	124.0	22.8	53.0
	20.0	197.0	243.0	38.6	68.0
16	5.0	46.0	64.0	14.6	29.0
	10.0	97.0	109.0	24.2	39.0
	20.0	200.0	230.0	41.6	69.0
32	5.0	47.0	51.0	15.0	31.0
	10.0	100.0	110.0	22.8	42.0
	20.0	206.0	265.0	42.6	66.0
64	5.0	49.0	58.0	15.8	31.0
	10.0	103.0	117.0	22.4	57.0
	20.0	212.0	233.0	42.8	68.0
128	5.0	51.0	51.0	17.0	30.0
	10.0	107.0	124.0	23.6	54.0
	20.0	220.0	273.0	42.4	74.0

In case of the averaging problems (Barycenter, Entropic Barycenter, Median), the parameters of the invariant distributions are the dimension d and the number of distributions n_{σ} , taking values from sets $d \in \{3, 5, 10, 20, 50\}$ and $\{3, 5, 10, 20\}$,

respectively. The number of iterations for each method is averaged for 5 random initializations of the distributions Σ_i , which are i.i.d., drawn from the Wishart distribution $W(\text{Id}, d)$. The entropic regularization parameter in the Entropic Barycenter problem is set to $\gamma = 0.001$ and the smoothing parameter in the Median problem is set to $\varepsilon = 0.001$. In all three experiments, the iteration proceeds until the cost converges to the minimum up to the tolerance of $\epsilon = 10^{-10}$. As for the hyperparameters of the method, for Barycenters and Entropic barycenters, they are the same as for the KL problem. For the Median problem, a broader range of relaxations and regularizations was considered, namely $l_{\text{inf},\text{max}} \in \{0.1, 5.0, 15.0\}$ and $\beta_k \in \{1.0, 5.0, 10.0\}$. The mean number of steps taken by each method with the best set of hyperparameters, is given in Table 4. We can see that BWRAM always provided acceleration compared to plain Picard iteration, in fact more than an order of magnitude in certain cases. Riemannian methods are also outperformed in most cases, the exception being the results for the Median problem in dimension $d = 50$, where RGD is superior. We note however, that the performance of BWRAM in that case is still comparable.

Table 4: Mean number of iterations for the three averaging problems: Barycenter, Entropic Barycenter and Median. The best result for each pair of (d, n_σ) is given in bold.

d	n_σ	Barycenter				Entropic Barycenter				Median			
		BWRAM	Picard	RCG	RGD	BWRAM	Picard	RCG	RGD	BWRAM	Picard	RCG	RGD
3	3	5.4	6.2	31.6	14.4	4.4	6.6	15.8	8.8	12.8	27.0	31.0	30.3
	5	7.0	9.8	29.0	16.6	5.8	10.6	12.2	9.0	13.8	26.5	24.5	21.5
	10	6.8	8.6	28.6	15.8	4.8	10.4	16.4	9.8	13.4	23.3	22.4	15.8
	20	6.6	9.0	26.2	15.2	5.0	9.2	13.4	10.0	13.3	22.9	26.1	16.3
5	3	7.4	9.8	32.4	18.0	6.4	8.8	14.2	9.0	23.2	72.1	32.5	33.3
	5	7.2	9.6	34.8	18.2	5.6	8.2	15.8	9.8	13.5	46.1	24.5	17.2
	10	7.4	10.6	38.4	18.8	6.0	9.0	17.0	10.6	11.2	41.8	21.3	16.6
	20	7.2	10.0	36.0	19.0	5.0	9.4	18.4	10.8	10.0	39.3	22.1	14.8
10	3	8.6	13.6	26.4	19.2	7.0	14.2	9.0	8.6	11.9	120.9	30.8	25.2
	5	9.0	13.8	33.4	20.4	6.2	13.2	14.0	11.2	10.3	94.1	26.7	18.7
	10	8.8	13.8	40.6	22.6	6.6	11.0	15.6	12.6	10.4	89.7	22.7	15.6
	20	8.0	11.2	39.4	22.0	5.4	11.4	16.2	11.0	9.8	82.8	16.5	13.5
20	3	10.6	20.6	34.6	23.8	7.8	23.2	11.2	11.4	11.8	245.7	28.5	23.9
	5	11.2	19.0	36.6	21.6	7.0	23.8	12.2	11.0	11.3	206.0	30.5	19.7
	10	10.0	17.0	44.6	22.8	7.0	19.4	15.2	12.2	10.8	192.8	27.5	18.5
	20	8.8	13.4	44.8	21.8	6.8	15.8	18.0	12.4	10.6	177.5	14.8	14.5
50	3	13.4	26.4	37.2	30.8	8.6	23.4	16.0	14.0	28.4	707.5	32.2	28.0
	5	12.8	23.8	50.2	29.2	8.6	28.8	21.8	14.6	26.5	601.3	35.1	22.8
	10	11.2	18.6	44.4	27.4	7.0	22.4	21.0	14.4	25.5	506.9	44.3	25.8
	20	9.2	14.2	44.0	26.4	6.4	15.8	19.8	13.8	20.5	461.2	40.5	23.5